PERGAMON

Journal of Structural Geology 26 (2004) 47–69

JOURNAL OF STRUCTURAL GEOLOGY

www.elsevier.com/locate/jsg

The influence of grain boundary fluids on the microstructure of quartz-feldspar mylonites

Neil S. Mancktelow[a,*], Giorgio Pennacchioni[b]

[a]*Geologisches Institut, ETH-Zentrum, CH-8092 Zürich, Switzerland*

[b]*Dipartimento di Geologia, Paleontologia e Geofisica, Università di Padova and CNR—Istituto di Geoscienze e Georisorse (Sezione di Padova), Italy*

Received 15 August 2002; received in revised form 17 April 2003; accepted 24 April 2003

Abstract

Quartz-rich domains in pre-Alpine, water-deficient, amphibolite facies (510–580 °C, 250–450 MPa), pegmatite mylonites from Mont Mary (MM), western Alps, preserve a fine dynamically recrystallized grain size, without significant annealing, despite the high synkinematic temperatures and subsequent static greenschist facies Alpine overprint. The microstructure is dramatically different from more typical water-rich amphibolite facies mylonites, such as from the Simplon Fault Zone in the central Alps, where the recrystallized grain size is on the millimetre-scale. The difference reflects the dominant strain-induced recrystallization mechanism: (1) progressive subgrain rotation and grain boundary bulging for the dry MM examples; and (2) fast grain boundary migration for the wet Simplon examples. The grain boundary microstructure imaged with SEM is also very different, with most grain boundaries in the dry MM samples lacking porosity, whereas grain boundaries in the wet samples are decorated by a multitude of pores. Quartz grain boundaries from both wet and dry samples are locally coated by thin (100's of nanometres), possibly amorphous, silica films. Despite the differences in microstructure, the crystallographic preferred orientations (CPOs) of quartz-rich domains from both areas are very similar. Water-deficient conditions hinder grain boundary mobility and thereby modify the dominant recrystallization mechanism(s) but apparently have little influence on the intracrystalline slip systems, as reflected in the CPOs (strong *c*-axis Y maxima). In MM mylonites, both K-feldspar and plagioclase (An_{33-38}) dynamically recrystallize, consistent with the inferred metamorphic conditions. Under water-deficient conditions, mid- to lower-crustal rocks can deform heterogeneously under transitional ductile-brittle conditions at high differential stress (for MM ca. 300–500 MPa, as estimated for dry Mohr–Coulomb failure) and preserve this high-stress microstructure, because of the low mobility of dry grain boundaries.

Keywords: Quartz; Feldspar; Deformation; Microstructure; Mylonites; Crystallographic preferred orientation (CPO); Fluid-rock interaction

1. Introduction

Quartz and feldspar are the most common minerals in the crust and overwhelmingly dominate in acidic magmatic rocks. On subsequent deformation under elevated temperatures and pressures, these rocks may develop localized shear zones now marked by quartz-feldspar mylonites (e.g. Burg and Laurent, 1978; Lister and Price, 1978; Berthé et al., 1979; Ramsay and Allison, 1979). The deformational microstructure of these two minerals depends primarily on temperature, strain rate and water activity (Jaoul et al., 1984; Kronenberg and Tullis, 1984; Ord and Hobbs, 1986; Tullis and Yund, 1987, 1989; Hirth and Tullis, 1992; Gleason and Tullis, 1995; Kohlstedt et al., 1995; Dunlap et al., 1997; Stipp et al., 2002a,b; and many others). Because the differential stress dependence on temperature is exponential, whereas the dependence on strain rate is linear (Newtonian viscous) or less than linear (power-law creep), temperature is generally considered to have the most important effect. The onset of crystal plastic behaviour in quartz is usually taken to occur around 280–300 °C (e.g. Sibson et al., 1979; Van Daalen et al., 1999, Stöckhert et al., 1999) and the transition in dominant dynamic recrystallization mechanism from subgrain rotation to grain boundary migration generally at around 400 °C (e.g. Urai et al., 1986; Mancktelow, 1990). A considerably higher temperature for this transition at around 550 °C was reported by Stipp et al. (2002a,b), who considered the process in terms of variation in strain rate. The initiation of crystal plastic deformation

* Corresponding author. Tel.: +41-1-632-3671; fax: +41-1-632-1030.
E-mail address: neil@erdw.ethz.ch (N.S. Mancktelow).

0191-8141/03/$ - see front matter © 2003 Elsevier Ltd. All rights reserved.
doi:10.1016/S0191-8141(03)00081-6

and dynamic recrystallization of feldspar is usually reported to occur with the change from greenschist to amphibolite facies conditions at around 500 °C (e.g. Vidal et al., 1980; Olsen and Kohlstedt, 1985; Tullis and Yund, 1987; Pryer, 1993). Quartz microstructures in mylonites have also been used as a paleopiezometer, based on the dependence of dislocation density, subgrain size and recrystallized grain size on differential stress (e.g. Twiss, 1977; Etheridge and Wilkie, 1979; Weathers et al., 1979; Kohlstedt and Weathers, 1980; Ord and Christie, 1984; Hacker et al., 1990, 1992; Gleason and Tullis, 1995). However, these piezometers are not yet accurately calibrated.

Natural observations do not always support a straightforward correlation of deformation microstructures with temperature, and extreme variability in recrystallized grain size is sometimes observed in high temperature mylonites from different locations. Most high temperature quartz mylonites are coarse grained (>100 μm, e.g. Stipp et al., 2002a, fig. 3h; Kleinschrodt and Duyster, 2002, figs. 3 and 4) and show evidence of extensive grain boundary migration. Particularly for upper amphibolite to granulite facies conditions, the microstructure may be annealed, with nearly straight grain boundaries. For fast grain boundary migration, grain size is often only limited by the width of individual quartz ribbons abutting layers of differing composition. Individual secondary phases (feldspar, sillimanite, garnet, etc.) may be totally enclosed (e.g. Kleinschrodt and Duyster, 2002, figs. 3 and 4) and do not necessarily pin grain boundaries. However, other examples (e.g. Passchier, 1985), as well as the ones considered here, have a much finer recrystallized grain size (<25 μm). Since the temperature is similar for these fine- and coarse-grained examples, some other parameter must exert a controlling influence. The finer grain size is unlikely to be solely an effect of higher strain rate, both because of the weak dependence of flow stress on strain rate in the power-law creep field and because feldspar shows crystal-plastic behaviour in both cases.

This study argues that the amount, distribution and composition of fluids on the grain boundaries are the controlling factors. To support this hypothesis, a comparison is made between quartz-rich mylonites developed under different metamorphic conditions: water-rich greenschist to amphibolite facies mylonites from the Simplon Fault Zone (central Alps) and both water-deficient, pre-Alpine, upper amphibolite facies mylonites and water-rich, Alpine, greenschist facies mylonites from the Dent Blanche/Mont Mary nappes (western Alps). The comparison is based on the grain microstructure as observed in normal thin sections, backscatter and secondary electron SEM images of polished surfaces, secondary SEM images of broken surfaces and, for quartz, on the crystallographic preferred orientation (CPO).

The quartz microstructure of the water-deficient amphibolite facies Mont Mary mylonites is similar to the greenschist facies mylonites from both Simplon and Mont Mary, but very different from the water-rich amphibolite facies mylonites of the Simplon area (and from other water-rich, sillimanite-bearing shear zones, e.g. Musumeci, 2002). In contrast, the quartz CPO is similar for amphibolite facies mylonites from Simplon ('wet') and Mont Mary ('dry'), as is the feldspar microstructure. These comparisons suggest that water activity has a more marked effect on intercrystalline mechanisms (especially grain boundary mobility, e.g. Urai et al., 1986) than on intracrystalline glide. SEM imaging of grain boundaries and particularly the distribution of fluid-filled pores is used to support this hypothesis.

2. Geological setting

2.1. Mont Mary and Dent Blanche

The Mont Mary (MM) and the Dent Blanche (DBL) are composite tectonic units of the western Alps (Canepa et al., 1990). They belong to the upper Austroalpine domain (Ballèvre et al., 1986), forming the top of the Alpine nappe pile. The upper unit of MM and of the DBL (Valpelline unit) consist of a pre-Alpine high-grade metamorphic complex including paragneisses (Qtz–Grt–Bt–Sil–Pl–Kfs),[1] amphibolites (Hbl–Pl ± Cpx ± Grt), Di-Grt-bearing marbles and minor pods of Spl-Amph-bearing ultramafics. Overprint of these pre-Alpine protoliths by Alpine deformation and metamorphism is weak and non-pervasive, being mainly restricted to localized discrete greenschist facies mylonites. The other tectonic units of the MM and DBL, primarily composed of Tertiary sediments (Roisan Zone) and granitoids (Arolla unit, DBL), underwent the same Alpine P–T–t path as the paragneiss units considered here, but the Alpine overprint is pervasive (Canepa et al., 1990; Pennacchioni and Guermani, 1993).

In the MM upper unit, pre-Alpine amphibolite-facies mylonites derived from paragneiss were described by Pennacchioni and Cesare (1997). These mylonites overprint the main pre-Alpine fabric and the synmylonitic mineral assemblage is Qtz–Bt–Ms–Pl–Grt–Sil–Graph. The metamorphic conditions during mylonitization were estimated at 510–580 °C and 250–450 MPa, under water-deficient conditions. 'Dry' conditions were suggested to explain: (i) the association of mylonites with ductilely deformed pseudotachylytes, indicating cyclic brittle instabilities during the mylonitic deformation; (ii) the very fine grain size of dynamically recrystallized mylonitic quartz, which indicates a high synkinematic differential stress; and (iii) the sluggish kinetics of metamorphic reaction and the overall (regional) good preservation of the pre-Alpine metamorphic assemblage. Similar observations have been made by Passchier (1985) on water-deficient mylonites from the Pyrenees.

The rocks studied in this work are quartz-feldspar mylonites developed from pegmatites. They form layers, up to several metres in thickness, transposed parallel to the

[1] Abbreviations of mineral names follow Kretz (1983).

mylonitic foliation of the adjacent paragneiss mylonites, which were the mylonites described in Pennacchioni and Cesare (1997). Pegmatite mylonites show a strong S–L fabric. Locally, highly stretched fabrics (L > S) to L-type fabrics predominate. Synmylonitic sheath folds, with fold axes parallel to the mineral stretching lineation, are frequent. A characteristic sharp compositional banding is present, with alternating millimetre-thick layers of quartz and feldspar.

Fifteen different pegmatite mylonite samples were studied (mmS76-90). Several thin sections were prepared from each sample for optical microscope observation, as well as polished slabs and broken chips for SEM study.

For comparison, two samples (DBL 1514, 1537) of quartz-rich mylonites inside greenschist facies Alpine phyllonites developed from high-T pre-Alpine paragneisses (Valpelline unit) were analysed. The phyllonites form a continuous horizon, outlining the tectonic contact with the Arolla granitoid mylonites, with a thickness on the order of a few tens of metres. The transition from phyllonites to high grade pre-Alpine paraschists with no Alpine overprint occurs rapidly, over distances of <50 m. Phyllonites consist of fine-grained Qtz, Ms, Chl, Ab and Ep. Further details on these Alpine phyllonites can be found in Pennacchioni and Guermani (1993).

2.2. Simplon

The Simplon quartz mylonites developed from practically monomineralic veins in the Simplon Fault Zone of the central Alps. This structure is a major Neogene low-angle normal fault along which rocks from the footwall were exhumed and cooled from maximum temperatures of 550–600 °C (> 20 km depth) to near-surface conditions of less than 100 °C (Mancktelow, 1985, 1990; Grasemann and Mancktelow, 1993). Along the trend of the fault, the amount of footwall exhumation increases from north to south: maximum temperatures in the footwall to the north did not exceed ~300 °C whereas they were ~600 °C in the south. This regional transition allows a direct comparison of mylonite microstructures developed from lower greenschist to upper amphibolite facies conditions in a water-rich environment (as evidenced by extensive hydrous retrogression of anhydrous minerals, such as garnet, staurolite and kyanite).

3. Microstructure from optical and SEM backscattered electron observations

3.1. Mont Mary

The pegmatite mylonites show a sharp compositional banding resulting from deformation and grain size reduction of primary quartz, plagioclase and K-feldspar (Fig. 1a). Quartz domains are effectively monomineralic, whereas feldspar-rich layers locally have a polyphase composition, in the case of K-feldspar due to dynamic recrystallization of two-phase perthites (see Fig. 2a and b below) and in the case of plagioclase due to subsequent (mainly static) retrograde mineral growth (Figs. 1a and 2c and d).

Quartz layers consist of fine-grained recrystallized aggregates (Qtz_2) alternating with monocrystalline, high aspect ratio (up to 150:1) ribbons (Qtz_1; Fig. 1b and e). The microstructure of Qtz_2 exhibits some variability in different samples. In *XZ* sections (i.e. parallel to lineation, L_m, and orthogonal to foliation, S_m), the mylonites typically show slightly to strongly elongate Qtz_2 grains, defining a SPO subparallel or slightly oblique (<30°) to S_m (Fig. 1b and c; e.g. Simpson and Schmid, 1983; Law et al., 1984, 1986). In some cases, the microstructure is clearly bimodal (mmS82, mmS86, mmS89; Fig. 1c) with relatively coarse-grained (several 10's of micrometres) elongate grains ($Qtz_{2,1}$) mantled by ultra-fine-grained (2–5 μm), polygonal aggregates of equant grains ($Qtz_{2,2}$). Slightly coarser (mean grain size <25 μm) $Qtz_{2,2}$ aggregates may extensively replace $Qtz_{2,1}$ domains (e.g. Figs. 1d and 7a), resulting in a $Qtz_{2,2}$ aggregate with domainal extinction inherited from the precursor $Qtz_{2,1}$ texture (cf. Pauli et al., 1996). Optically, $Qtz_{2,1}$ grains have sutured and/or stepped boundaries (Fig. 1c), but the grain boundaries are often indistinct under the microscope, because the $Qtz_{2,2}$ grain size is much less than the thin section thickness. In only one sample (mmS90; Fig. 1e) is a foam texture consisting of small (10–30 μm) polygonal grains (alternating with Qtz_1 ribbons) developed without any evidence for a precursor $Qtz_{2,1}$.

Qtz_2 recrystallized grains show a well-developed CPO, as revealed by a strong gypsum plate effect, with distinct bands of similar crystallographic orientation arranged parallel to S_m (Figs. 1b and e and 7a). This banding of the CPO reflects a clear host control by precursor Qtz_1 ribbons on the orientation of new Qtz_2 grains (Pauli et al., 1996), as can be seen in regions where the recrystallization is incomplete. It follows that the width of the CPO banding is similar to the width of Qtz_1 ribbons (Fig. 1e). The Qtz_1/$Qtz_{2,1}$ optical microstructure (Fig. 1b) is typical of recrystallization by progressive subgrain rotation (e.g. Poirier and Nicolas, 1975; regime 2 of Hirth and Tullis, 1992; fig. 3e of Stipp et al., 2002a; fig. 7e of Stipp et al., 2002b), whereas the optical microstructure of incipient $Qtz_{2,1}$ to $Qtz_{2,2}$ recrystallization is similar to that usually associated with grain boundary bulging recrystallization (Bailey and Hirsch, 1962; Means, 1981; Urai et al., 1986, fig. 3; Stipp et al., 2002b, fig. 7d). This is typified by (1) sutured $Qtz_{2,1}$ grain boundaries, (2) very fine new $Qtz_{2,2}$ grain size (reported in the range 5–25 μm by Stipp et al., 2002a), and (3) only a small volume fraction of new grains (generally less than 20%, Stipp et al., 2002a). However, in MM mylonites a transition to higher volume fractions of fine new $Qtz_{2,2}$ grains can be observed and in many examples a predominantly unimodal fine (<25 μm) grain size is observed (e.g. Figs. 1d and 7a–c).

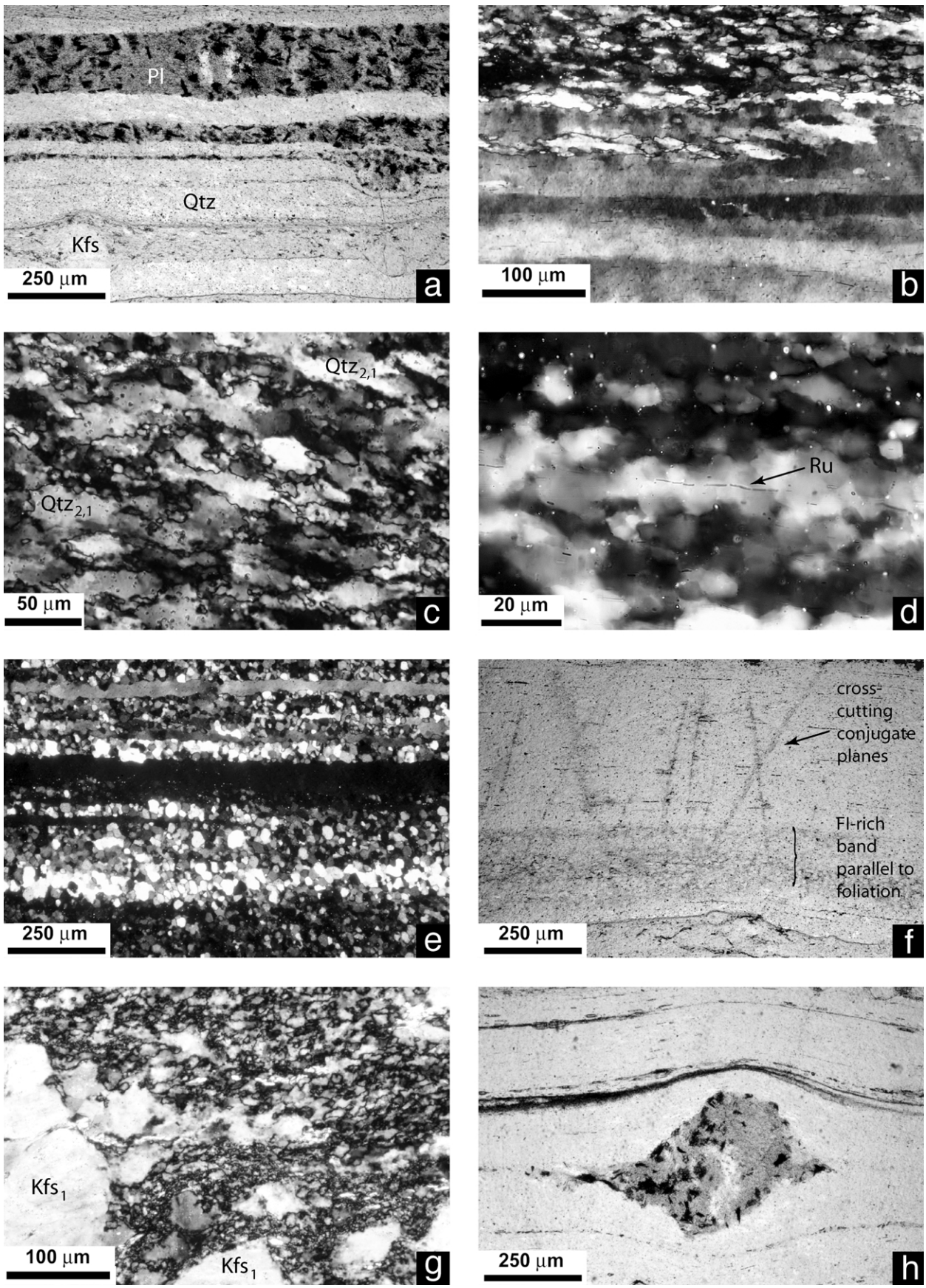
Pl
Qtz
Kfs
250 μm
a
100 μm
b
Qtz2,1
Qtz2,1
50 μm
c
Ru
20 μm
d
250 μm
e
cross-cutting conjugate planes
Fl-rich band parallel to foliation
250 μm
f
Kfs1
100 μm
Kfs1
g
250 μm
h

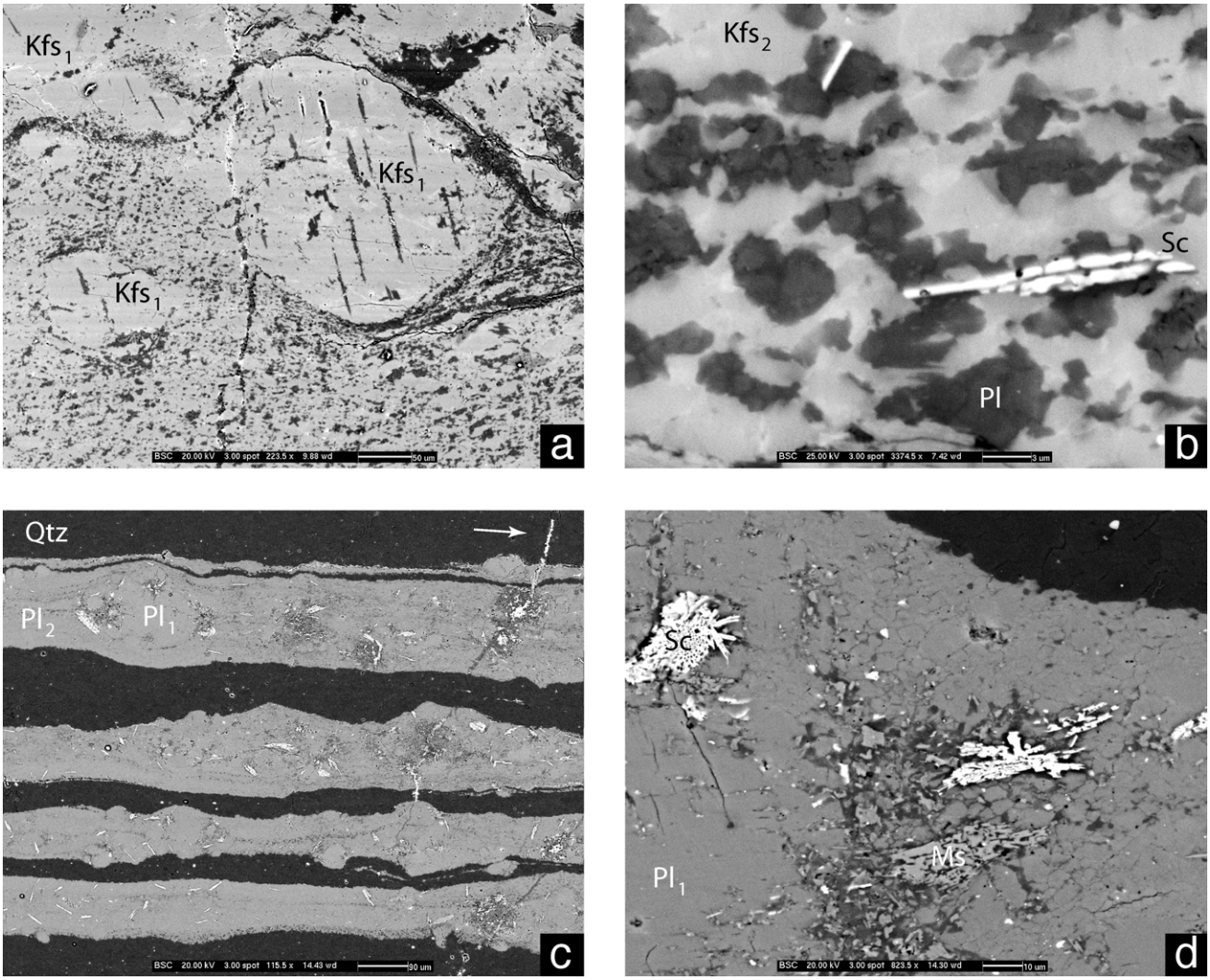

Fig. 2. SEM backscatter images of feldspar layers in MM mylonites. All sections *XZ*. (a) Kfs porphyroclasts with straight perthite lamellae surrounded by a recrystallized intergrown Kfs_2 + Pl matrix. Kfs is light grey, Pl (ca. An_{40}) is dark grey. Sample mmS88; scale bar 50 μm. (b) Detail of the recrystallized matrix. Sc is white, Kfs light grey, Pl (ca. An_{40}) dark grey, with darker thin rims of more albitic composition. Scale bar 3 μm. (c) Recrystallized Pl_2 (light grey), with relict Pl_1 porphyroclasts, and Qtz (dark grey) layers. Randomly oriented Ms (lighter grey) and Sc (white) within Pl layers are in some cases clearly related to crosscutting fractures (e.g. arrow in upper right). Sample mmS81; scale bar 90 μm. (d) Detail showing local enhanced retrogression with growth of Ms (light grey), Sc (white) and grain boundary rims of albite (darker grey) on the polygonal aggregate of Pl_2. Relict Pl_1 porphyroclast is indicated. Sample mmS81; scale bar 10 μm.

Fig. 1. Photomicrographs of the optical microstructure of quartz-feldspar mylonites from Mont Mary. All sections *XZ* (perpendicular to foliation, parallel to lineation), sense of shear sinistral. (a) Typical alternating quartz (Qtz), plagioclase (Pl) and K-feldspar (Kfs) layers, with porphyroclasts transitional to recrystallized mantles and tails; plagioclase layers show extensive static alteration to scapolite (black randomly oriented sheaves) and fine white mica (dark grey); plane polarized light. (b) Quartz ribbons recrystallizing to $Qtz_{2,1}$, showing a clear oblique SPO consistent with the sinistral sense of shear; crossed polars. (c) Recrystallization of $Qtz_{2,1}$ (with an oblique SPO) to $Qtz_{2,2}$; sinistral sense of shear, crossed polars. (d) Boudinaged rutile needles parallel to S_m, showing slight change in orientation across subgrain and new $Qtz_{2,1}$ grain boundaries; the lack of offset or large rotation precludes any significant component of grain boundary sliding; bright spots in the quartz aggregates are grain boundary solid inclusions; crossed polars. (e) Quartz monocrystalline ribbons alternating with recrystallized quartz layers with a unimodal foam texture and extinction banding; bright grains have *c*-axes close to the plane of the thin section (i.e. the *XZ* plane); crossed polars. (f) Type A fluid inclusion distributions occur either as crosscutting, often conjugate planes, transecting bands of all three minerals (Qtz, Pl, Kfs), or as distributed bands parallel to S_m; plane polarized light. (g) Grain size reduction of Kfs_1 porphyroclasts to Kfs_2; note the similarity of the Kfs_2 microstructure to that of $Qtz_{2,1}$/$Qtz_{2,2}$ in (c); crossed polars. (h) Plagioclase δ-shaped porphyroclast system showing partial alteration to white mica (grey) and radiating scapolite (black); plane polarized light. All examples are from sample mmS80E_3, except for (e), which is from mmS90.

Small boudinaged needles of rutile are abundant inside quartz ribbons and Qtz_2 aggregates. When inside monocrystalline ribbons, rutile is arranged in well-aligned rows of microboudins perfectly parallel to the *XY* plane (i.e. ribbon margin/S_m), but locally slightly oblique to *X*. Elongations recorded by microboudin separation are on the order of 30–50%. In the recrystallized Qtz_2 aggregates, rutile occurs as trains of microboudins, undulating slightly in their orientation, or as dispersed segments that can no longer be assigned to a single original parent grain. In this case, their orientation shows some scattering around a mean parallel to S_m, but still with a very strong unimodal shape preferred orientation parallel to S_m. In Qtz_2 aggregates, rutile needles often show minor kink-like rotation across Qtz_2 grain boundaries of similar magnitude to the minor crystallographic misorientation between quartz grains developed by subgrain rotation recrystallization from a single earlier grain (Fig. 1d). The small misorientation between single rutile needles in adjacent recrystallized grains (Fig. 1d) and in Qtz_2 aggregates relative to adjacent ribbons precludes significant grain boundary sliding or granular flow.

Under the optical microscope, two different types of fluid inclusions (FIs) are irregularly distributed in quartz layers. A first type (type A) is very small (<1 μm) and individual FIs appear as opaque dots even at high magnifications (50–100 ×). These FIs (Fig. 1f) occur in two forms: (i) as trails along fractures inclined at a high angle to the mylonitic foliation, crosscutting the grain boundaries and the compositional layering; and (ii) along grain boundaries, with a patchy distribution in the recrystallized domains or, more commonly, concentrated along bands parallel to S_m bounded by FI-free domains. There is no apparent change in Qtz microstructure between domains rich or poor in these FIs. Trails of type (i) are visible to the naked eye transecting quartz ribbons on polished samples. In *XY* sections, they form at a high angle to the mylonitic lineation. FIs of a second type (Type B) are relatively large (up to several micrometres in diameter) and faceted. These are present along the grain boundaries of quartz close to the contact with feldspar layers and in the feldspar domains themselves, where they form patchy concentrations giving a dusty appearance to the feldspar. Type B FIs also show alignment along high angle fractures.

Some Qtz_2 domains are clouded with birefringent solid granules (mica?) decorating the grain boundaries. Granule-rich bands parallel to foliation have sharp contacts against granule-free bands. Similar to FIs, they also decorate fractures at high angles to foliation.

K-feldspar layers include numerous porphyroclasts (Kfs_1) set in a very fine-grained matrix (ca. 3–5 μm) of apparently recrystallized grains of dominantly Kfs_2 (Fig. 1a). The clast/matrix ratio is variable but usually rather high. Grain size reduction initially occurs by dismembering of large (millimetre–centimetre) Kfs_1 clasts along conjugate sets of fractures/microshear zones outlined by thin horizons of new ultra-fine grains (e.g. Debat et al., 1975; Passchier, 1982). Large Kfs_1 clasts show strong intracrystalline deformation, as indicated by undulose to patchy extinction and very thin flame perthites (Fig. 2a), often arranged in en-échelon arrays along conjugate microshear zones (cf. Passchier, 1982). However, Kfs_1 also shows extensive grain size reduction to aggregates of dominant Kfs_2 resembling recrystallization domains. Locally, these domains have an optical microstructure almost identical to the transition from $Qtz_{2,1}$ to $Qtz_{2,2}$ described above (Fig. 1g). One important difference compared with Qtz is the lack of precursor ribbon grains, indicating that Kfs does not undergo significant intracrystalline dislocation creep prior to grain size reduction. During deformation and recrystallization, Kfs_1 clasts dismember and move apart across the intervening domains of newly formed fine Kfs_2 grains derived from the same parent clast, but often maintain a similar crystallographic orientation even when widely separated. With increasing strain and increasing ratio of matrix to clasts, feldspar layers are stretched to 'pinch and swell' domains, with swells consisting of Kfs_1 porphyroclasts and the intervening neck domains composed of the fine-grained aggregates. This microstructure can develop further to δ-shaped porphyroclast systems with connected thin long tails of fine-grained material.

The matrix aggregates of Kfs_2 have a SPO parallel to S_m and, in some cases, show a weak to strong gypsum plate effect (mmS88, 89). Optically, the fine-grained (ca. 3–5 μm) aggregates are colourless but show some relief contrast, indicating a polyphase composition. In fact, SEM backscattered electron images reveal that the matrix is polymineralic (Fig. 2a and b) and composed of dominant Kfs_2 (with identical composition to Kfs_1: Table 1) associated with a K–Na–Ca–Al–Si phase (EDS analysis), with variable Ca/Na. A similar EDS composition is also detected for 'perthite' lamellae in the Kfs_1, which suggests that this K–Na–Ca–Al–Si phase represents a mixed Pl + Kfs composition. The maximum Ca/Na is similar to that of the recrystallized Pl domains (see below). Randomly oriented sheaves of scapolite locally overgrow these mineral domains (Fig. 2b). In SEM backscatter images, thin darker rims are developed on the Pl intergrown with Kfs (Fig. 2b), which may reflect minor albitic alteration associated with this late (Alpine) static retrogression. Optically, only minor to accessory white mica is present inside K-feldspar layers (in marked contrast to the plagioclase domains described below). This white mica in Kfs layers is very localized and mainly present along fractures oriented at a high angle to S_m. Some of these fractures are post-kinematic to the main foliation-forming event, as they clearly crosscut the mylonitic fabric and sometimes extend into adjacent Qtz layers. The white mica in these fractures has a variable grain size (from a few tens to 500 μm) and is randomly oriented. Other, better oriented Ms occurs as: (i) thin seams defining discontinuous S-type planes along Kfs_1 fractures (or less frequently along the

Table 1
Electron microprobe analyses of K-feldspar porphyroclasts and adjacent fine-grained tails from sample mmS80

Sample	Clast_1	Clast_1	Tail_1	Tail_1	Clast_2	Clast_2	Tail_2	Tail_2
K-feldspar electron microprobe analyses								
SiO_2	63.49	63.45	62.82	63.41	64.17	62.78	63.75	64.76
Al_2O_3	18.85	18.88	18.32	18.51	18.88	18.82	18.69	18.28
CaO	0.07	0.26	0.16	0.02	0.02	0.04	0.00	0.01
Na_2O	0.80	0.78	0.50	0.85	0.92	0.47	0.57	0.57
K_2O	16.05	16.11	16.54	16.01	15.77	16.32	16.32	16.13
Total	99.27	99.48	98.34	98.79	99.75	98.42	99.34	99.75
Feldspar endmembers								
Orthoclase	0.926	0.920	0.949	0.925	0.917	0.957	0.949	0.949
Albite	0.070	0.068	0.044	0.075	0.082	0.041	0.051	0.051
Anorthite	0.003	0.012	0.008	0.001	0.001	0.002	0.000	0.001

conjugate fracture sets in the porphyroclasts) or tangential to porphyroclasts; (ii) small scattered pressure shadows around porphyroclasts; and (iii) very thin layers parallel to S_m commonly present at the boundary of Kfs layers. White mica seams of type (i) discordantly cut recrystallized Kfs_2 aggregates.

Plagioclase shows recrystallization to very fine-grained Pl_2 (≤ 5 μm) followed by alteration to scapolite (Sc), white mica and albite-rich plagioclase (Fig. 1a). In mylonites, Pl_2 often extends as tails/necks between rounded Pl porphyroclasts and gives the Pl layer a pinch-and-swell profile that can develop further to δ-shaped porphyroclast systems (Fig. 1h). Where preserved, Pl_2 aggregates show a clear gypsum plate effect, indicating a strong crystallographic preferred orientation. The composition of the fine recrystallized Pl_2 grains in the tails is identical to the composition of the precursor Pl_1 porphyroclasts (i.e. An_{33-38}; Table 2). Pl_1-Pl_2 domains generally show an extensive to complete replacement by Ms–Ab–Sc, but a few samples show only weak alteration (mmS80, 81, 84 and 89; Fig. 2c). In these less altered samples, Pl_2 aggregates have a local 'microcataclastic' microstructure with Pl_2 grain boundaries sealed by a thin rim of Na-rich plagioclase (Fig. 2d). This alteration is commonly related to late fractures crosscutting the compositional layering of the quartz-feldspar mylonites (upper right of Fig. 2c). Sc forms randomly oriented poikilitic to skeletal lamellae and sheaves (Figs. 1a and h and 2c and d). Replacement is mainly static (e.g. Fig. 1a and h) and often occurs along high-angle microcracks, but aggregates of Ms oriented parallel to the foliation are also observed. It is worth noting that the two samples mmS81 and mmS84 in which the alteration of Pl is weakest (e.g. Fig. 2c) both show a fine-grained, dominantly $Qtz_{2,2}$ microstructure as described above. However, there is no apparent correlation between the Qtz microstructure and the degree of Pl alteration. Strongly altered Pl domains are mainly composed of a fine Ms–Ab intergrowth, with small islands of relict Pl containing corroded Sc. Locally, Ep + Ab develops as a further alteration stage. The uniformly distributed partial alteration along even quite thin Pl_2 tails (e.g. Fig. 1a) suggests that the plagioclase layers were preferential conduits for water access along layering during subsequent (Alpine?) metamorphism. The access across layering was probably provided by microcracks (e.g. Fig. 2c), now healed and outlined by fluid inclusions as in Fig. 1f.

Sillimanite is locally present inside pegmatite mylonites. It is commonly boudinaged to rectangular grains with their long axes parallel to S_m and with Ms present within the microboudin necks. Some thin Ms layers subparallel to S_m

Table 2
Electron microprobe analyses of plagioclase porphyroclasts and adjacent fine-grained tails from sample mmS80 (Clast_1 and Tail_1) and mmS89

Sample	Clast_1	Tail_1	Tail_1	Clast_2	Tail_2	Tail_2	Clast_3	Tail_3
Plagioclase electron microprobe analyses								
SiO_2	57.21	59.98	59.45	58.02	60.08	58.64	58.72	59.06
Al_2O_3	25.69	25.64	26.07	25.58	25.24	26.20	26.45	26.07
CaO	7.43	7.13	7.29	8.15	6.96	8.37	7.94	8.02
Na_2O	7.69	7.97	7.99	7.50	7.90	7.47	7.47	7.68
K_2O	0.42	0.17	0.08	0.13	0.09	0.10	0.33	0.05
Total	98.44	100.88	100.87	99.37	100.27	100.77	100.90	100.88
Feldspar endmembers								
Orthoclase	0.023	0.009	0.004	0.007	0.005	0.005	0.018	0.003
Albite	0.637	0.663	0.662	0.620	0.669	0.614	0.619	0.632
Anorthite	0.340	0.328	0.334	0.373	0.326	0.380	0.363	0.365

are associated with Sil, but Sil transformation is generally very incomplete.

3.2. Valpelline phyllonites

The optical microstructure of the Alpine retrograde mylonites (Fig. 3a and b) is distinctly different from that of the MM pegmatite mylonites. Although they also show quartz ribbon grains (Fig. 3a), there is only a single generation of recrystallized grains, which appears to have formed by subgrain rotation, consistent with development under lower greenschist metamorphic conditions. The recrystallized grain size (Fig. 3b) is of similar order to that of $Qtz_{2,1}$ grains in the pre-Alpine mylonites (i.e. 30–50 μm), but coarser than the pre-Alpine $Qtz_{2,2}$ grains. Recrystallized aggregates show a strong CPO and a domainal extinction inherited from the orientation of the precursor ribbon structure (Fig. 3a). Ribbons show saw-tooth boundaries, deformation lamellae and subgrain polygonization, particularly toward the rims (Fig. 3a). At high magnification, ultra-fine (<2–3 μm) fluid inclusions are ubiquitous as opaque dots along Qtz_2 grain boundaries. In monocrystalline ribbons, deformation lamellae are often outlined by dusty stripes of densely spaced fluid inclusions. In the studied samples of these Alpine retrograde mylonites, post-kinematic fractures crosscutting mylonitic layering have not been observed.

3.3. Simplon

Quartz microstructures from the Simplon Fault Zone show the influence of increasing temperature both into the footwall and from NW to SE, reflecting different amounts of total exhumation (Mancktelow, 1985, 1987a,b, 1990). Relevant to this study is the transition in dominant recrystallization mechanism from subgrain rotation to grain boundary migration. This transition occurs together with the first appearance of synkinematically stable biotite in the retrogressive mylonite fabrics, corresponding to temperatures around 400 °C (e.g. Winkler, 1979; Bucher

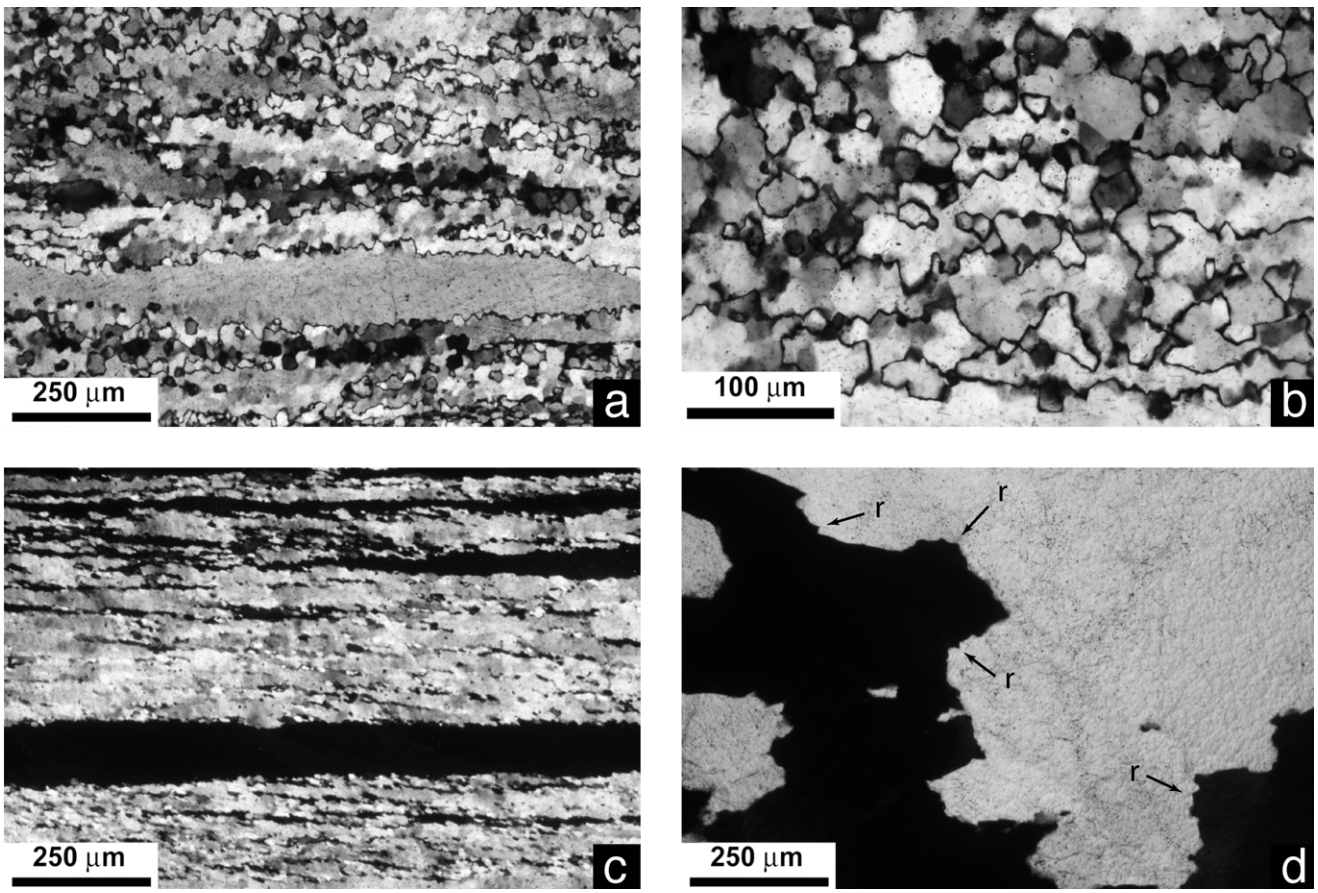

Fig. 3. Photomicrographs of optical microstructure of water-rich quartz-feldspar mylonites from Valpelline and Simplon. All sections *XZ* (perpendicular to foliation, parallel to lineation), sense of shear sinistral, crossed polars. (a) Quartz ribbons and recrystallized new grains forming a foam texture in an Alpine, greenschist facies mylonite from Valpelline. Note the finely serrated grain boundary to the ribbon grain, indicative of slow migration. Sample DBL 1514. (b) Close-up of the recrystallized Qtz_2 grains. (c) Ribbon grains and recrystallized Qtz_2 showing an oblique SPO; greenschist facies mylonite from the Simplon Fault Zone. Sample SP54 from near Simplon village. (d) Large recrystallized grain size due to fast grain boundary migration in wet amphibolite facies quartz mylonite from the Simplon Fault Zone in Val d'Isorno (sample SP136). Probable rhomb crystal faces are indicated with (r).

and Frey, 1994). At lower temperature, quartz microstructures are dominated by elongate ribbon grains transitional at their boundaries into recrystallized Qtz_2 domains (Fig. 3c). Qtz_2 grains show an oblique SPO consistent with the sense of shear and a banding in their CPO reflecting development from precursor ribbon grains (Fig. 3c). Preserved ribbon grains have their *c*-axes near, but seldom strictly parallel, to the *Y* axis, so that they appear dark grey to black under crossed polars (Fig. 3c; Mancktelow, 1987a, 1990). The dominant recrystallization mechanism is progressive subgrain rotation (regime 2 of Hirth and Tullis, 1992). Overall, the optical microstructure is very similar to that observed in the quartz-rich layers of the pre-Alpine MM mylonites. Indeed, some less common quartz microstructures from the Simplon Fault Zone (Mancktelow, 1987b) show completely analogous $Qtz_{2,1}$ to $Qtz_{2,2}$ recrystallization as was described above for the MM mylonites. With the transition to synkinematic amphibolite facies conditions in the wet Simplon Fault Zone, grain boundary migration becomes the dominant recrystallization mechanism and grain coarsening is dramatic. Millimetre-sized grains show typical serrated grain boundaries (Fig. 3d), reflecting development of perfect rhomb crystal faces on the grain boundary scale (arrows on Fig. 3d; see also Mancktelow et al., 1998). This microstructure is in stark contrast to the MM samples deformed under comparable temperatures in the upper amphibolite facies, which do not show any evidence of grain coarsening due to grain boundary migration recrystallization.

4. SEM secondary electron imaging of the grain boundary microstructure

4.1. Mont Mary

Secondary electron imaging of broken surfaces under the SEM is a simple but powerful technique for direct observation of grain boundary microstructure (for details of the method see Hippertt (1994a,b) or Mancktelow et al. (1998)). MM samples have been studied on broken surfaces approximately parallel to *XY* and *XZ* sections. On ca. *XZ* sections, some samples (e.g. mmS80, mmS88) show a bimodal grain size. In detail, the microstructure consists of larger (several tens of micrometres in length) elongated $Qtz_{2,1}$ grains, defining a SPO inclined to S_m, and a mantle of small (<5 μm in diameter) equant $Qtz_{2,2}$ grains (Fig. 4a and b). The broken surface tends to form a hachured intergranular fracture across $Qtz_{2,1}$ grains, whereas $Qtz_{2,2}$ grains mainly separate along grain boundaries (Fig. 4a–d). In samples mmS80 and mmS88, the mantle of $Qtz_{2,2}$ grains is only one to three grains thick (Fig. 4b–d). On both ca. *XY* and *XZ* sections, $Qtz_{2,2}$ grains in most cases have developed well-formed polygonal crystal faces and the grain boundaries are completely free of decoration (Fig. 4c–f), with no ridges or voids along triple junctions. In contrast, other areas show local fine-scale grain boundary pores, which sometimes occur over domains encompassing many grains. Pores may be crystallographically controlled, with regular geometric shapes (triangular to hexagonal) depending on the orientation of the grain face relative to the crystal axis, or they may be more rounded (Figs. 4f and 6a and b). The regular shapes are identical in geometry to typical etch pits. They often show a preferred spacing (like nodes of a regular grid) with a unimodal or, less frequently, bimodal distribution of pore size, with the pore size itself generally <0.5 μm. Overall, this grain boundary geometry is very similar to that observed in greenschist facies mylonites from the Simplon Fault Zone (e.g. Fig. 6e; see also fig. 4 in Mancktelow et al. (1998)), except that grain boundary porosity is much more pervasively developed in the water-rich Simplon examples.

Kfs_2 generally has a finer grain size than that for quartz (Fig. 4g and h) but its grain boundary microstructure is otherwise identical. It develops a polygonal foam-like mosaic with most grain boundaries free of decoration but with isolated pockets of very fine pores, similar to those described above for quartz. Although Kfs_2 grains are often concentrated on narrow, fracture-like zones transecting large porphyroclasts, the grain shape and surface features are generally indistinguishable from those of quartz (compare Fig. 4e and h), with no evidence for cataclasis or fracturing at the grain scale (Fig. 4h).

Plagioclase also recrystallizes to a very fine grain size (2–4 μm; Fig. 5a and b), but in contrast to K-feldspar also commonly involves retrograde reaction to white mica (± late scapolite; see Fig. 1a and h). As a result, recrystallized plagioclase bands are not monomineralic and the intergrowth with mica results in a much more open pattern of interlocking grains, with important interconnected porosity (Fig. 5b). Later (probably Alpine) hydrous retrogression of plagioclase-rich layers can lead to complete replacement by randomly oriented rosettes of white mica and albite. This growth clearly postdates the mylonitic microstructure.

Secondary electron SEM imaging of polished surfaces of water-deficient MM mylonites reveals a tight structure free of almost any pores. This is in marked contrast to Simplon examples, which can show connected porosity on the scale of millimetres (see fig. 3 in Mancktelow et al., 1998).

4.2. Valpelline

Alpine greenschist facies mylonites show quartz grain boundary microstructures that are very different from those described for the pre-Alpine MM mylonites. In contrast to the smooth, well-formed quartz grain faces in MM mylonites, with only a limited number of regularly arranged pores, quartz grain boundaries from Alpine retrograde samples show a ubiquitous rough topography (Fig. 5c–f). This microstructure is locally very similar to the ‘ridge and valley’ grain boundary structure described by Hippertt

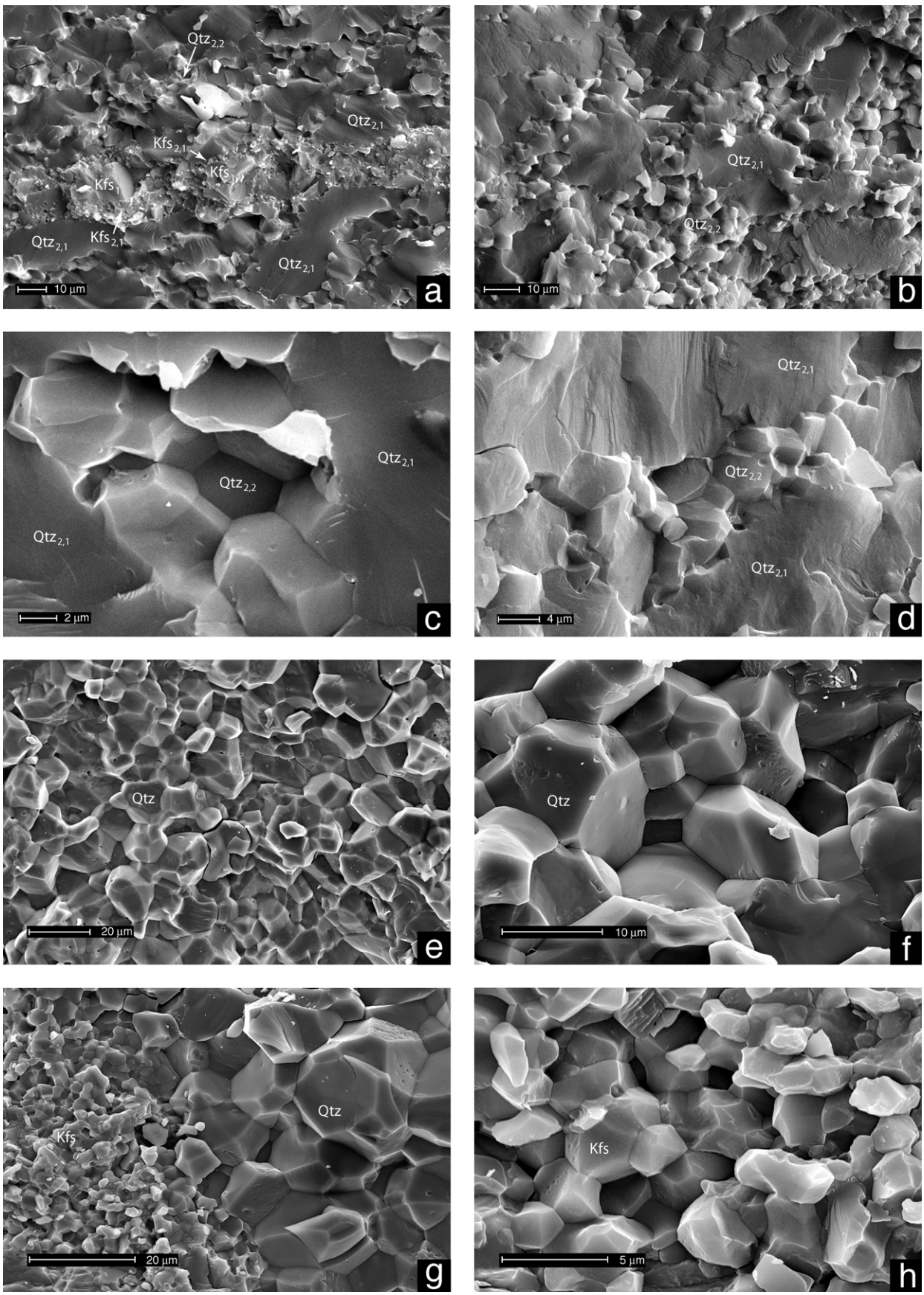
Qtz2,2
Qtz2,1
Kfs2,1
Kfs1
Kfs1
Qtz2,1
Kfs2,1
Qtz2,1
10 µm
a
Qtz2,1
Qtz2,2
10 µm
b
Qtz2,1
Qtz2,2
Qtz2,1
2 µm
c
Qtz2,1
Qtz2,2
Qtz2,1
4 µm
d
Qtz
20 µm
e
Qtz
10 µm
f
Qtz
Kfs
20 µm
g
Kfs
5 µm
h

(1994b, fig. 5a and b) and the 'island-channel' network structure considered by Gratz (1991) and Den Brok (1998). Grain boundaries are only to a first approximation flat. In detail, they have a strongly 'corroded' aspect with submicron sized bulges and depressions. These topographic irregularities do not have a regular size or distribution along the grain face, but they do commonly show some crystallographic control on morphology, with a tendency to develop second-order crystal facets. In some cases, this grain boundary decoration does not correspond to any open porosity but in fact closely matches the corresponding negative shape of the opposing grain surface (arrow on Fig. 5d) and may represent an irregular dissolution surface (cf. Den Brok, 1992). The SEM observations demonstrate that the grain boundaries are strongly serrated at the submicron-size even though in thin section the quartz appears as a perfectly polygonal foam microstructure. Other grain boundary surface features resemble structures described by Den Brok (1992), with channel networks of irregular geometry often showing alignments along partially healed microfractures (arrow on Fig. 5f; cf. Den Brok and Spiers, 1991). This irregular channel network is associated with a finer-grained true porosity with a more regular pore size and distribution (Fig. 5f). Such features were locally also observed in the Simplon retrogressive mylonites, but not in the water-deficient upper amphibolite facies mylonites of MM.

4.3. Simplon

Samples for SEM study from the Simplon Fault Zone were broken along approximately *XY* sections (i.e. parallel to mylonitic foliation). The SEM microstructure of samples showing grain size reduction by subgrain rotation recrystallization is very similar to that observed in MM examples, reflecting the similarities in optical microstructure. The one important difference is that grain boundary porosity is much more extensive in Simplon samples (e.g. see Fig. 6e; Mancktelow et al., 1998, figs. 2 and 4). As noted above, many grain boundaries from MM samples are almost pore-free, whereas this is rare in the Simplon samples. Larger-scale (>100 μm), connected porosity has also been observed in many Simplon samples, irrespective of the deformation temperature and dominant recrystallization mechanism (e.g. Mancktelow et al., 1998, fig. 3). Such large-scale porosity has never been observed in any of the high-grade shear zones from MM. The perfect crystal forms developed on migrating grain boundaries in the higher-grade Simplon samples (see fig. 5 of Mancktelow et al., 1998) have also not been observed in the MM samples.

4.4. Grain boundary films—MM and Simplon

One intriguing feature is common to both the amphibolite facies dry MM mylonites and the wet Simplon mylonites: in each case there is evidence for local development of grain boundary films (Fig. 6). Qualitative analysis by EDS under the SEM indicates that the films are effectively pure (amorphous?) SiO_2, though the very small thickness (on the scale of a few 100's of nanometres) makes it impossible to fully exclude the quartz host grain substrate from the analyses. Rounded pores in these films do not penetrate into the underlying grain, resulting in a flattened pancake-shaped pore geometry with the depth of penetration more-or-less constant irrespective of pore size (Fig. 6a). Films on some grain surfaces coat and obscure earlier porosity (Fig. 6b–d). Locally these thin films appear to 'neck-down', like grease between two separating plates, into complex brain and worm-like patterns (Fig. 6c, d and f–h; see also Mancktelow et al. (1998, figs. 6–8) and the discussion therein). There is a tendency for the worm-like structures to form ridges along grain triple points (centre of Fig. 6d, f and g). The fact that the films coat existing porosity pits, together with the development of intricate patterns clearly related to separation of grain boundaries (e.g. Fig. 6c and d), indicates that the films, as currently observed, are late-stage features. However, they could also have been present (and continually modified) during progressive deformation.

5. Crystallographic preferred orientation (CPO) in quartz

The CPO of quartz-rich domains in several representative MM pegmatite mylonite samples is given in Fig. 7, together with photomicrographs of the optical microstructure. The complete CPOs determined by X-ray texture

Fig. 4. SEM secondary electron images of broken surfaces of dry Mont Mary quartz-feldspar mylonites. (a) Thin K-feldspar band (with Kfs_1 porphyroclasts embedded in tails of fine recrysallized Kfs_2 grains) surrounded by larger elongate $Qtz_{2,1}$ grains with mantles of fine polygonal $Qtz_{2,2}$, *XZ* surface (mmS80). (b) Irregular $Qtz_{2,1}$ surrounded by fine, equigranular $Qtz_{2,2}$, *XZ* surface (mmS80). (c) Enlargement of the transition from $Qtz_{2,1}$ to $Qtz_{2,2}$ grains as seen in (b). Note the polygonal form, the fine grain size (2–3 μm), and the typical pore-free grain boundaries, *XZ* surface (mmS80). (d) Transition from $Qtz_{2,1}$ to $Qtz_{2,2}$ new grains. Note again the general lack of porosity on the new grain boundaries, *XZ* surface (mmS88). (e) Typical foam structure of recrystallized quartz grains developed in mmS90 (see Fig. 1e). Note the low overall porosity on most grain boundaries, *XY* surface. (f) Enlargement of the typical foam structure of mmS90, showing the equilibrium grain shapes and generally tight structure without pervasive porosity. The porosity distribution is, however, heterogeneous—although most grain boundaries are almost pore-free, local pockets exist where grain boundaries are covered in scattered fine pores, e.g. in the centre-right of the photograph (see also Fig. 6a and b), *XY* surface. (g) Recrystallized quartz and finer-grained K feldspar, showing the marked difference in grain size but otherwise similar grain microstructure, *XY* surface (mmS90c). (h) Enlargement of the K-feldspar domain in (g), showing the similar polygonal grain shape as for quartz and the generally tight, pore-free grain boundaries, with only local development of isolated pores on two-grain boundaries, *XY* surface (mmS90c).

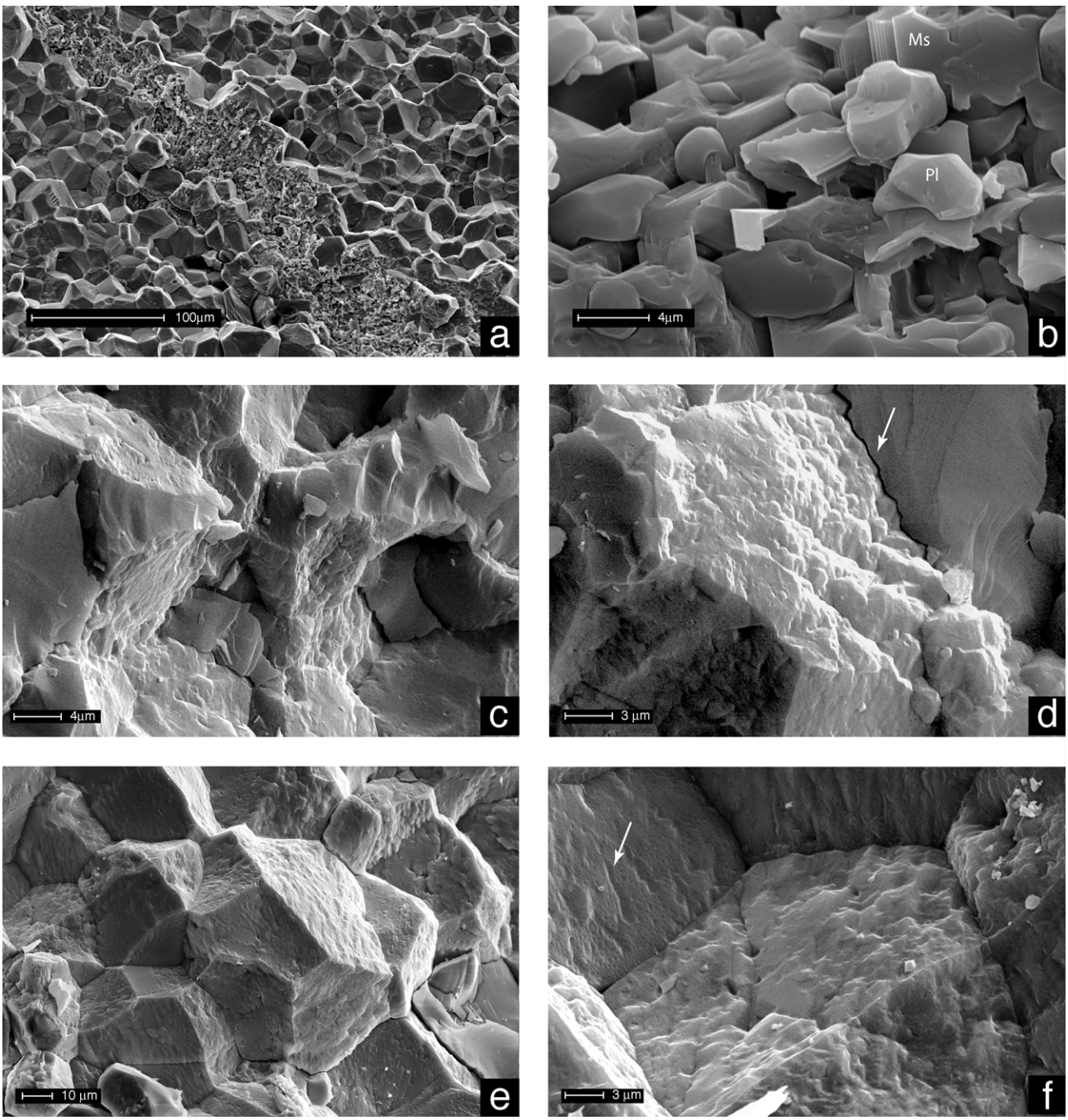

Fig. 5. SEM secondary electron images of broken surfaces of pre-Alpine dry (MM, a, b) and Alpine wet (DBL, c–f) quartz-feldspar mylonites. (a, b) Pre-Alpine MM pegmatite mylonites. (a) Recrystallized plagioclase band (defining the foliation) in a matrix of recrystallized quartz. Sample mmS90c. (b) Enlargement of the central area of (a), showing the interconnected porosity at a grain scale that is typical when white mica is present, indicating locally enhanced permeability and higher fluid activity, reflected in the retrograde hydration of Pl to Ms (mmS90c). (c–f) Quartz grain boundaries in greenschist facies Alpine mylonites (c,d:DBL1514; e,f:DBL1517). (c) Typical pervasive rough aspect of grain boundaries in recrystallized aggregates of polygonal quartz. (d) Detail of the "ridge and valley" microstructure of a quartz grain boundary, showing a rough topography controlled by second-order crystal facets; note that the grain boundary forms match closely with those on opposite grains (arrow on upper right part of photo). (e) Grain boundary roughness in 'foam grains' of sample DBL1537. (f) Relatively coarse, irregular to faceted grain boundary roughness associated with a fine more regular porosity; note the alignment of faceted cavities (e.g. as indicated by the arrow), probably representing healed microcracks.

goniometry for four different samples are plotted in Fig. 7a–d and the cumulative *c*-axis orientation of monocrystalline ribbons measured in different mylonites with the universal stage is given in Fig. 7e. The degree of preferred orientation is strong for both ribbons and recrystallized grains, with a *c*-axis maximum near the central intermediate *Y* axis (with some tendency for spreading within a partial girdle) and an ⟨*a*⟩ axis concentration at the periphery, at a small synthetic angle to the stretching lineation. The CPO of mmS90 (Fig. 7d) is somewhat different in that it is closer to a kinked single girdle distribution. Within this single girdle, there is a strong bimodal concentration of the *c*-axes, with one maximum parallel to *Y* and another at the periphery oblique to the foliation and lineation, in a sense synthetic with the (sinistral) sense of shear. This peripheral concentration in mmS90 would suggest an additional component of basal ⟨*a*⟩ slip (e.g. Schmid and Casey, 1986). The microstructure of mmS90 is also rather atypical, consisting of ribbons and recrystallized Qtz_2 grains developing a well-equilibrated foam texture (Fig. 1e), without the $Qtz_{2,1}$ to $Qtz_{2,2}$ progression more common in the other samples (e.g. Fig. 1c). The peripheral maximum of mmS90 is due to some of the recrystallized Qtz_2 grains (those with maximum interference colours near white under crossed polars, other Qtz_2 grains have *c*-axis orientations near *Y* and low order interference colours) and not to the ribbon grains, which show a consistent *c*-axis CPO close to the *Y* axis (Fig. 7e).

All the high-grade MM samples show a streaking-out in the distribution of the other crystallographic axes in a rotational sense around the central *c*-axis maximum. This is most clearly seen in the distribution of ⟨*m*⟩ and ⟨*a*⟩ axes and is more marked the stronger the concentration of *c*-axes in a single central maximum (i.e. for samples mmS83 and mms84; Fig. 7b and c). This distribution is identical to that observed in two 'atypical' samples from the Simplon mylonites (Mancktelow, 1987b), which also show the bimodal $Qt_{2,1}$ to $Qtz_{2,2}$ optical microstructure typical of MM mylonites. This similarity is considered further in the discussion section below.

The pre-Alpine high-grade MM samples in general show only a weak tendency to develop an oblique girdle although, as noted in Mancktelow (1987a), goniometer methods that measure a volumetric average tend to mask these effects compared with grain-by-grain methods (optical or electron backscatter diffraction—EBSD). In contrast, the measured retrograde Alpine Valpelline mylonite DBL1514 (Fig. 8) shows a kinked asymmetric crossed-girdle pattern typical of greenschist facies conditions (Lister, 1977; Law et al., 1984, 1986; Law, 1986, 1987, 1990; Schmid and Casey, 1986), as is also well exemplified by the greenschist facies Simplon mylonites (Mancktelow, 1987a, 1990). In contrast with the dry MM samples, the wet Valpelline sample (Fig. 8) does not show a concentration of *c*-axes parallel to the *Y* axis, typical of prism ⟨*a*⟩ slip, but rather maxima more typical for rhomb or basal ⟨*a*⟩ slip.

The results establish that the CPOs of both the high-grade pre-Alpine MM and retrograde Alpine Valpelline (DBL) mylonites are in good accord with the synmylonitic metamorphic conditions, suggesting that mechanisms of intracrystalline glide are also typical of the metamorphic conditions. It is the microstructure that is inconsistent and this largely reflects the dominant recrystallization mechanism rather than the dominant intracrystalline deformation mechanism. This observation, namely that the measured CPOs of the natural examples considered in this study are largely independent of the variation in microstructure (and therefore in implied recrystallization mechanism), differs from the experimental results of Gleason et al. (1993), who recognized a strong dependence.

6. Discussion

6.1. Deformation and recrystallization mechanisms in quartz and feldspar

For the dry, amphibolite facies MM mylonites, the synkinematic evolution of quartz involves the following microstructural sequence: (i) elongation of the original coarse Qtz grains to ribbon grains and development of deformation bands (i.e. elongate bands within grains with slight differences in extinction) approximately parallel to the elongation direction; (ii) recrystallization of those deformation bands that are less well-oriented for slip to $Qtz_{2,1}$ aggregates forming elongate domains of similar orientation (cf. Pauli et al., 1996), whereas deformation bands well-oriented for prism slip (i.e. with *c*-axes near parallel to the *Y* axis; Fig. 7e) remain as monocrystalline ribbons; (iii) second stage recrystallization of $Qtz_{2,1}$ grains to finer grained aggregates of $Qtz_{2,2}$, involving a gradual transition from initial thin mantles (1–3 grains wide) to, in some cases, near complete development of a very fine-grained recrystallized $Qtz_{2,2}$ mosaic, while some ribbons remain unrecrystallized.

This observed sequence of microstructures would fit with a change in recrystallization mechanism with increased strain. In particular, the transition from $Qtz_{2,1}$ to $Qtz_{2,2}$ could indicate a change from dominant subgrain rotation to grain boundary bulging recrystallization, possibly reflecting an increase in differential stress due to decreasing temperature, higher strain rate or drier conditions. However, according to both natural (e.g. Stipp et al., 2002a,b) and experimental (e.g. Hirth and Tullis, 1992) observations, bulging recrystallization is unable to completely transform the precursor fabric to a fine-grained new fabric. In contrast, in our examples a pervasive fine-grained (<25 μm) microstructure is progressively developed and preserved. These fine quartz grains show a strong CPO with a *c*-axis *Y* maximum, generally considered typical of prism ⟨*a*⟩ glide and grain boundary migration recrystallization (cf. fig. 14 of Stipp et al., 2002b).

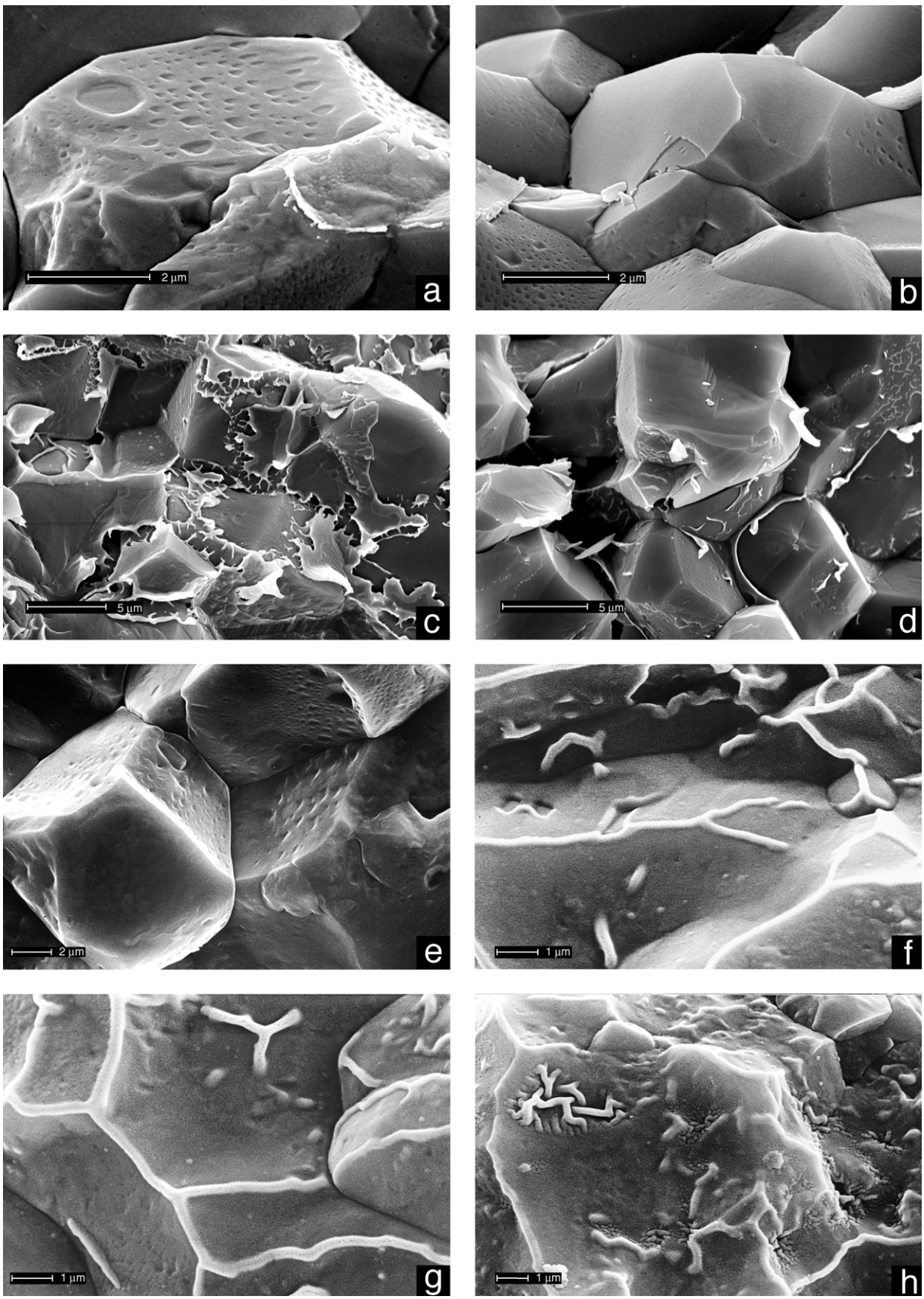
2 μm
a
2 μm
b
5 μm
c
5 μm
d
2 μm
e
1 μm
f
1 μm
g
1 μm
h

Fine new Kfs_2 grains occur both as mantles on Kfs_1 porphyroclast rims and along narrow microshear zones within the Kfs_1, as previously observed by Debat et al. (1975) and Passchier (1982). The general lack of grain boundary porosity (Fig. 4h) and the common strong gypsum-plate effect, indicating a strong CPO of new grains similar to the host porphyroclast, argues for dynamic recrystallization by progressive subgrain rotation and/or bulging rather than microfracture and rotation of clasts. The absence of a significant precursor elongation of the Kfs porphyroclasts is more consistent with bulging recrystallization. Comparable natural dynamic recrystallization of Kfs has been previously reported for both amphibolite facies (e.g. Vidal et al., 1980; Passchier, 1982; Pryer, 1993) and 'dry' eclogite facies (Altenberger and Wilhelm, 2000) conditions.

Deformation and recrystallization mechanisms in plagioclase are difficult to decipher unequivocally in the MM pegmatite mylonites because of subsequent retrogressive mineral growth during hydration. This preferential water infiltration parallel to thin Pl-bands in itself suggests that the grain boundary microstructure of the fine-grained 'recrystallized' Pl aggregate was more porous (and hence more permeable) than that for Qtz and Kfs bands. Kruse et al. (2000) describe two concurrent mechanisms for grain size reduction of Pl (An_{48-55}) porphyroclasts under conditions of ca. 700 °C and 900 MPa. Type-1 porphyroclasts in a 'soft orientation' for crystal-plastic slip recrystallized by progressive subgrain rotation and consequently the new grain orientations showed host control. Type-2 porphyroclasts in a 'hard orientation' were reduced in grain size by microfracturing and cataclasis and the recrystallized grains did not show host control. In MM samples, the strong gypsum-plate effect of both porphyroclasts and 'recrystallized' fine grains in Pl bands suggests a strong host control in MM samples and therefore a dominance of true subgrain rotation recrystallization. However, local microfracturing and rotation of clasts could still be important in developing connected porosity and therefore enhanced permeability. The lack of any change in composition (together with the observed host-control on crystallographic orientation) argues against significant dynamic neocrystallization driven by changing metamorphic conditions (P, T and water activity), but this was certainly important during later (largely static) retrograde reaction to Ms–Ab–Sc ± Ep (Fig. 2d). Overall, the observations are in accord with previous studies, with dominant subgrain rotation recrystallization under mid- to upper amphibolite facies conditions associated with little change in composition being supplanted by nucleation and growth of new grains of different composition under lower amphibolite to greenschist facies conditions (e.g. Fitz Gerald and Stünitz, 1993; Pryer, 1993).

6.2. Timing of the preserved microstructures

Several lines of evidence establish that the dominant microstructure in the MM pegmatite mylonites developed under high temperature (amphibolite facies) conditions. Firstly, the pegmatite mylonites are interleaved with paragneiss mylonites whose synkinematic conditions were estimated at ca. 550 °C (Pennacchioni and Cesare, 1997) and both pegmatite and paragneiss mylonites show the same stretching lineation and sense of shear. Secondly, the strong *c*-axis *Y*-maximum with an ⟨*a*⟩-axis maximum near the stretching direction, as determined for the MM pegmatite mylonites, is typical of quartz mylonites developed under upper greenschist to amphibolite facies conditions (e.g. Schmid and Casey, 1986; Mancktelow, 1990; Mackinnon et al., 1997). The only exception is the peripheral *c*-axis maximum shown by sample mmS90, which is largely defined by the recrystallized Qtz_2 grains. Thirdly, the dynamically recrystallized assemblage (Qtz, Kfs, An_{33-38}–Pl) indicates amphibolite facies conditions and there is little or no synkinematic alteration of these phases. Dynamic recrystallization of K-feldspar has only been described under amphibolite facies (e.g. 550 °C: Vidal et al., 1980; 530 ± 40 °C: Pryer, 1993) and eclogite facies (Altenberger and Wilhelm, 2000) conditions. In MM mylonites, deformation and recrystallization of K-feldspar is accompanied by minor development of flame perthite. Though flame perthite is usually formed under greenschist facies conditions (e.g. Pryer and Robin, 1995), it may also grow at higher (amphibolite facies) temperatures (e.g. Vernon, 1999). In this case, the Na required for growth of the flames may come from local redistribution of the precursor 'magmatic'

Fig. 6. SEM secondary electron images of grain boundary SiO_2 films and ridges on broken surfaces of Mont Mary and Simplon quartz-rich mylonites. (a–d) dry MM mylonites, (e–h) wet Simplon mylonites. (a) On this quartz grain boundary, the depth of penetration of rounded pores is the same, regardless of the pore size, suggesting that the boundary is covered by a thin film of more-or-less constant thickness and that the pores only penetrate this film but not the underlying grain (mmS90). (b) Thin silica film coating the grain boundary and earlier pores. A small segment of this film, without surface structure, has broken away in the centre of the image, revealing the pitted surface of the grain beneath. Typical inverse crystal shape pores, with the depth of penetration reflecting the size of the pore, are seen in the bottom left of the image, which contrast with the pores in (a) (mmS90). (c) Thin irregular silica film on quartz grain boundaries (EDS qualitative analysis yields only an SiO_2 peak), locally necking down to typical worm-like structures (mmS90). (d) Thin films coating quartz grain boundaries, with worm-like raised ridges on grain triple points in the centre of the image (mmS90). (e) Typical pore structure on quartz grain boundaries from greenschist facies water-rich mylonites from the Simplon Fault Zone. Note that in comparison to the water-deficient MM samples, porosity is much more extensive. Note also that for these crystallographically controlled pores, the depth of penetration is dependent on the pore size (SP54). (f) Silica worm-like ridges developed preferentially on quartz grain triple point junctions and clearly developed over pre-existing porosity similar to (e) (SP54). (g) Worm-like ridges on grain triple points (SP54). (h) Characteristic 'brain-like' geometry of ridges developed on two-grain interfaces (SP54).

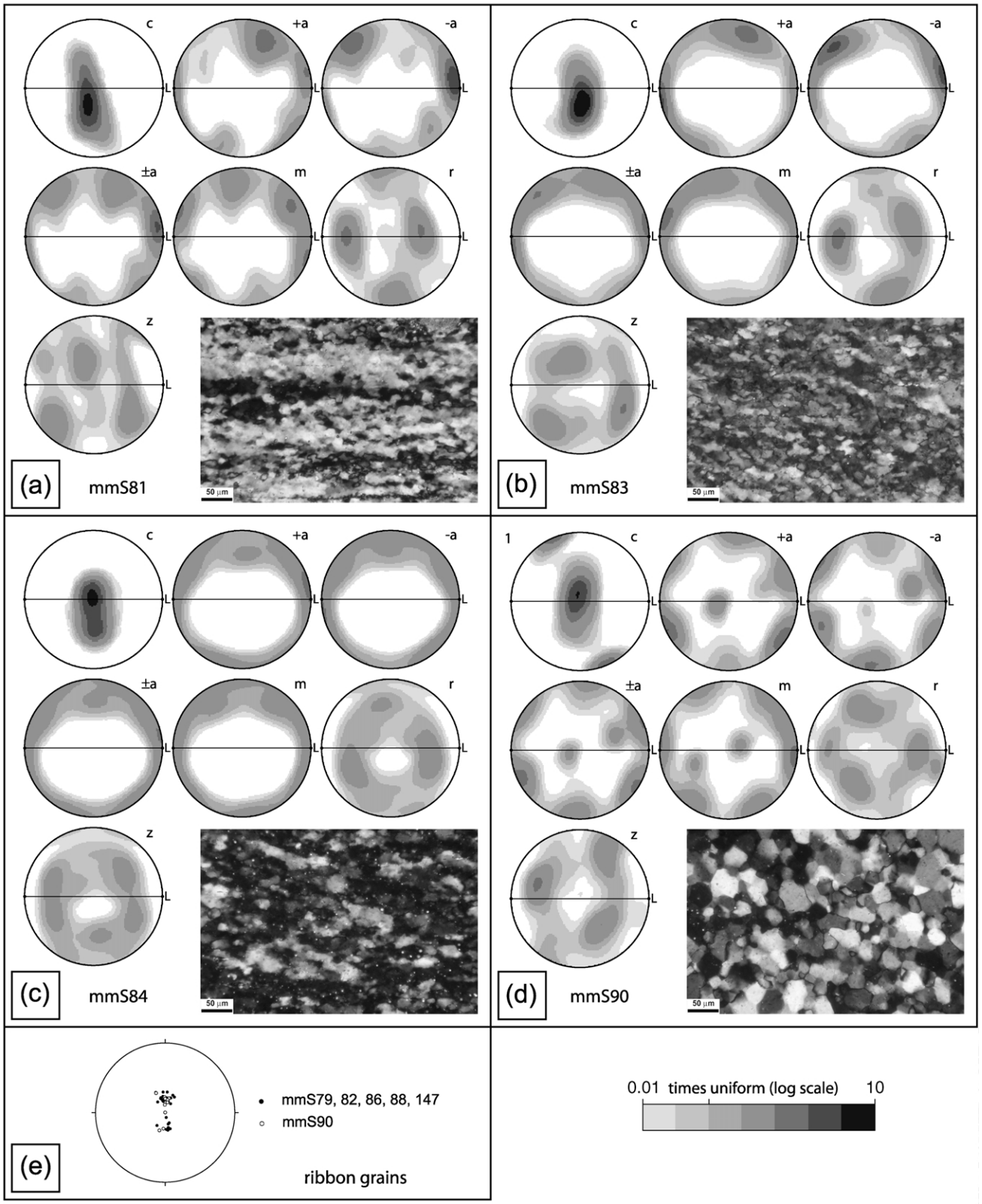

Fig. 7. Crystallographic preferred orientation (CPO) of quartz from MM water-deficient, high temperature mylonites, determined by X-ray texture goniometry (a–d) and cumulative *c*-axis orientation of quartz in monocrystalline ribbons measured optically with a universal stage (e). (a) mmS81; (b) mmS83; (c) mmS84; (d) mmS90; (e) open circles: mmS90; filled circles: mmS79, mmS82, mmS86; mmS88, mmS147. In all cases, the projection is into the upper hemisphere and the foliation is arranged EW and vertical, with the lineation horizontal. The sense of shear is sinistral (top-to-SE in the field). Contours spacing is logarithmic, ranging from 0.01 to 10 times a uniform distribution. Scale bar on all photomicrographs is 50 μm.

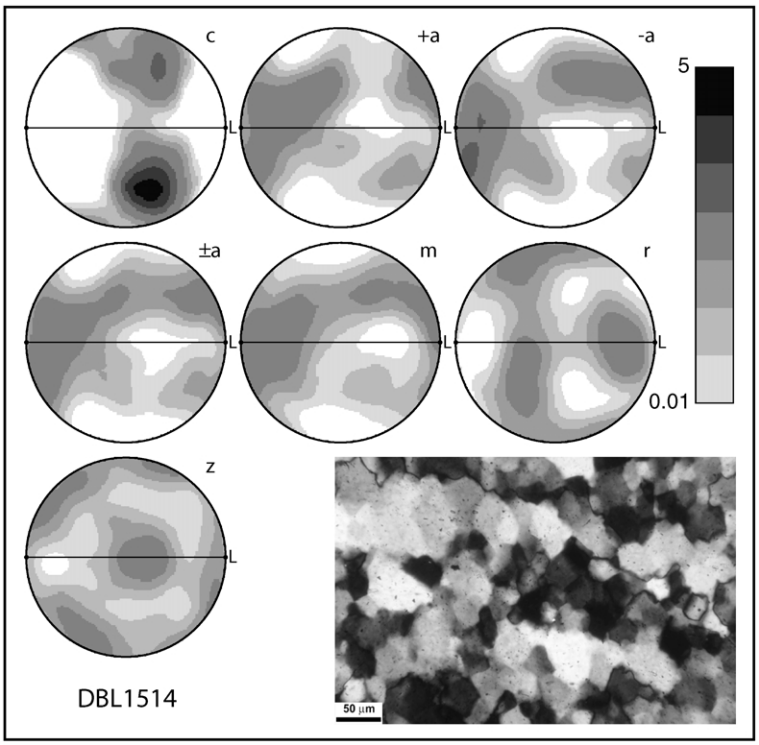

Fig. 8. Crystallographic preferred orientation of quartz sample DBL1514, a retrograde greenschist facies Alpine mylonite, determined by X-ray texture goniometry. The projection is into the upper hemisphere and the foliation is arranged EW and vertical, with the lineation horizontal. The sense of shear is sinsitral (top-to-NW in the field). Contours are logarithmic, ranging from 0.01 to 5 times a uniform distribution. Scale bar on the photomicrograph is 50 μm.

perthites present in the K-feldspar. The relatively high Ca content of plagioclase in both the 'perthites' and the recrystallized Kfs_2 supports this argument. Similarly, recrystallization without any significant change in composition of An_{33-38}-plagioclase is consistent with amphibolite facies metamorphic conditions, rather than the more albitic composition stable under lower greenschist facies.

Muscovite growth is mainly postkinematic, but minor oriented Ms also indicates that ductile deformation in part occurred during breakdown of Kfs, Sil and Pl. Oriented Ms fabrics are apparently late as they overprint feldspar recrystallization aggregates. However, they do indicate the same sense of shear as the main high-T kinematic indicators and could represent a late stage deformation stage of progressive mylonitic activity under falling T. Alternatively, Ms-bearing and Ms-absent domains may simply reflect microstructural domains with different water activities, related to synkinematic water-rich fluid partitioning in an overall water-deficient environment. Consistent with the first interpretation, a moderate- to lower-T (greenschist facies) reactivation of the early amphibolite facies Qtz aggregates could possibly explain the bimodal Qtz microstructure with mantles of $Qtz_{2,2}$ related to the later low-T deformation. In this case, the most extensive re-equilibration of Pl would be expected in the samples with the finest Qtz grain size (i.e. the strongest retrograde fabric reactivation). However, this is not true for samples mmS81-84, where a fine Qtz grain size is associated with a very weak alteration of Pl.

In summary, these arguments all support the development of the fine to ultra-fine grained dynamic recrystallization microstructure of Qtz, Kfs and Pl under high temperature (amphibolite facies) conditions and their preservation, without significant overprint (e.g. by annealing), during the subsequent pre-Alpine and Alpine tectonometamorphic history. The decoration of some grain boundaries by etch-pit like pores and locally by intricate grain boundary film structures must be coeval with or postdate this recrystallization. More tightly defined criteria to establish the time of their formation are lacking. It is unlikely that the fine detail of the grain boundary films as seen in Fig. 6c and d could have survived Alpine greenschist facies overprint and indeed some of the detail may even have developed during grain separation on breaking of the slabs for SEM observation (see discussion in Mancktelow et al., 1998). As discussed immediately below, the local development of porosity in MM mylonites observed under the SEM may reflect local heterogeneous infiltration of water-rich fluid during subsequent (Alpine) hydrous retrogression and not the water-deficient conditions under which the main microstructure developed.

6.3. Fluid infiltration

In MM pegmatite mylonites, secondary electron SEM imaging of broken surfaces from recrystallized Qtz domains has shown that the grain boundaries are either completely

free of decoration, with well formed planar crystal faces, or (more locally) strongly pitted, with regular arrangements of crystallographically-controlled pores. The regular pore shapes suggest a water-rich composition of the fluid phase (since CO_2 and CH_4 are poor solvents for SiO_2). Grain boundary fluids show a non-equilibrium distribution, being mainly located along grain faces instead of at three-grain junctions (e.g. Fig. 6b). This distribution has also been observed in several other studies of quartz in mylonites and seems to be the norm rather than the exception (Hippertt, 1994a,b; Mancktelow et al., 1998).

The SEM observation of fluid-rich and fluid-poor domains matches the optical observation of fluid-inclusion-free and fluid-inclusion-rich zones. The extremely fine size of type A grain-boundary fluid inclusions observed under the microscope (see Section 3.1) is consistent with the sub-micrometre-size grain-boundary porosity observed under the SEM. Therefore, linking the optical and SEM observations, it can be proposed that the grain boundary porosity observed in MM pegmatite mylonites is postkinematic, being associated with high angle fractures cross-cutting the mylonitic foliation (e.g. Figs. 1f and 2c and d). The postkinematic, late-stage character of fluid infiltration is supported by the absence of any significant microstructural difference between the fluid-free and the fluid-rich domains. This late fluid infiltration is most likely coeval with the partial to nearly complete retrograde replacement of plagioclase, involving hydration reactions to muscovite and scapolite and coeval growth of albite. Permeability was provided along the mylonitic layering by the porous structure of the Pl_2 aggregates (Fig. 5b) and across the layering by discrete fractures (Fig. 1f), now healed as trails of fine fluid inclusions. The distribution of fluid inclusions observed in quartz layers of MM mylonites and the rather pervasive retrograde static replacement of plagioclase indicate that fluid infiltration during metamorphism, in the absence of active ductile deformation, is rather effective.

6.4. Correlation of CPO and optical quartz microstructure for MM, Valpelline and Simplon

Two samples of quartz mylonites (out of several hundred) collected from the Simplon Fault Zone show the same $Qtz_{2,1}$ to $Qtz_{2,2}$ optical microstructure and CPO as the water-deficient high-grade MM mylonites (see Mancktelow, 1987b). The two known localities for these 'atypical' deformation fabrics in the Simplon area are widely separated (SP107/108 and SP140 on fig. 1 of Mancktelow (1987b)) and do not appear to reflect the usual NW–SE progression in deformation microstructure. It cannot be excluded that they represent 'fossil' fabrics that also developed under higher-grade metamorphic conditions (similar to those for the pre-Alpine MM) and were locally preserved during continued normal faulting and exhumation of the footwall. However, there is no good argument why conditions in the Simplon region should ever have been water-deficient.

All other measured CPOs from Simplon show patterns typical of the metamorphic conditions during deformation, i.e. kinked asymmetric *c*-axis girdles for lower to mid-greenschist facies transitional to a concentration of *c*-axes around the *Y*-axis for upper greenschist to amphibolite facies conditions (Mancktelow, 1987a, 1990). The transition roughly corresponds to the change from grain size reduction by subgrain rotation to grain coarsening by grain boundary migration during dynamic recrystallization. The sample measured from the Valpelline Alpine phyllonites (Fig. 8) also shows the kinked *c*-axis girdle pattern typical of greenschist facies conditions.

In contrast, the samples from MM show a strong *c*-axis maximum parallel to *Y*, indicating a dominant prism $\langle a \rangle$ slip system that is typical of amphibolite facies quartz mylonites (e.g. Schmid and Casey, 1986). Fig. 9 is a schematic diagram from Stipp et al. (2002b), which has been modified to show the correlation between CPO, recrystallization mechanism, temperature and grain size reported by these authors for the Tonale quartz mylonites. The range in deformation temperature of dry MM mylonites inferred from the synkinematic metamorphic paragenesis (510–580 °C; Pennacchioni and Cesare, 1997), together with the range in grain size observed in the finer-grained samples whose CPOs are presented in Fig. 7a–c (mmS81, 83, 84), are given as boxes on this figure. It is immediately clear that the CPOs of Fig 7a–c are in good accord with the temperature of deformation, but the grain size is an order of magnitude lower than would be expected, and more consistent with a bulging recrystallization mechanism. However, bulging recrystallization is not normally associated with a large volume fraction of recrystallized grains, whereas the MM mylonites are often extensively recrystallized to fine new grains ($Qtz_{2,2}$, e.g. see photomicrographs of Fig. 7).

In summary, although the optical Qtz microstructures of the dry amphibolite facies MM pegmatite mylonites are similar to those of the wet greenschist facies mylonites from Simplon and Valpelline, the CPO is quite different and typical of the amphibolite facies conditions under which they actually developed. Water activity has therefore had a marked effect on the grain microstructure, but apparently not on the dominant intracrystalline glide mechanism(s) and CPOs.

6.5. Development and preservation of a fine-grained microstructure under water-deficient conditions

The fine grain size of the high-grade MM quartz-feldspar mylonites reflects grain size reduction during recrystallization, without grain growth or subsequent annealing. This preservation is despite temperatures exceeding 500 °C during shear zone development and despite the later greenschist facies Alpine metamorphism that has locally

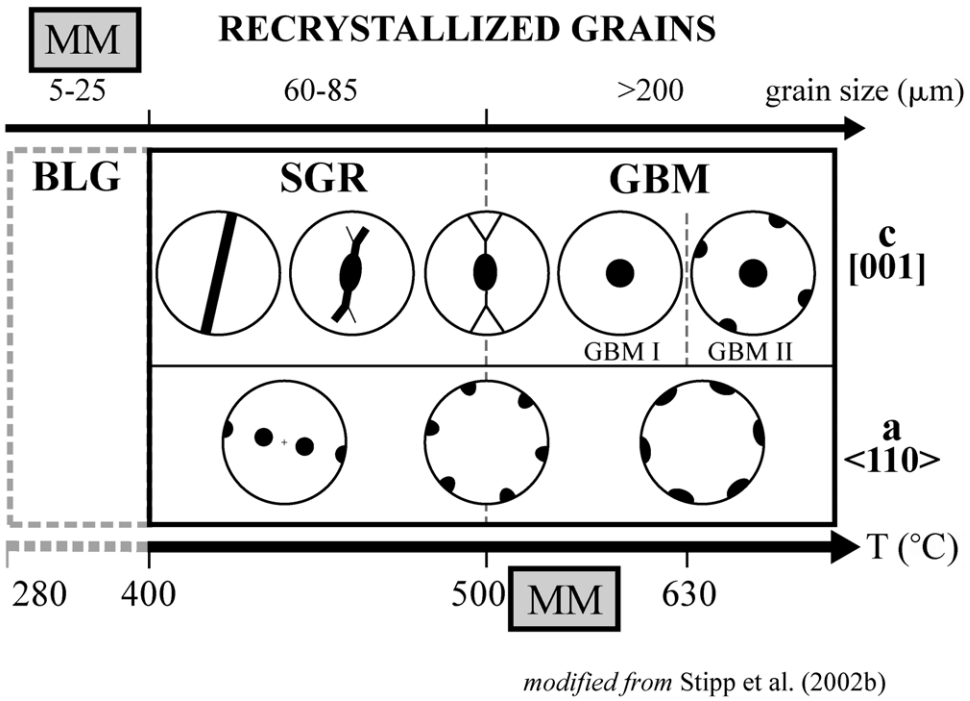

Fig. 9. Schematic diagram modified after Stipp et al. (2002b) showing the correlation between grain size, CPO and temperature inferred for the Tonale quartz mylonites. The upper and lower grey boxes represent the grain size range and estimated synkinematic temperature (Pennacchioni and Cesare, 1997) for the fine-grained dry MM mylonites whose CPOs are presented in Fig. 7a–c (mmS81, 83, 84).

produced random growth of white mica (Figs. 1a and h and 2d), scapolite (Figs. 1a and h and 2b–d) and epidote. Quartz grain sizes, which are in some cases less than 5 μm, were preserved throughout this long metamorphic history (e.g. Fig. 4). This preservation is in dramatic contrast to samples from the Simplon area, where shearing under similar PT conditions produced grain boundary migration recrystallization of quartz and final grain sizes on the scale of millimetres (Fig. 3d). However, the CPO of the MM samples is as expected for the metamorphic conditions—the parameter that has hindered grain growth in the MM examples and promoted it in the Simplon examples does not similarly affect the mechanisms of intracrystalline glide and consequent development of CPO. Since P and T conditions are similar, there has to be some other parameter that is responsible for the observed difference in grain microstructure. One possibility is a dramatic increase in strain rate related to a change in deformation mechanism. The very fine recrystallized grain size in the MM mylonites could be used to argue for superplastic behaviour, due to diffusion-accommodated grain boundary sliding. However, for simple shear, the stress is the same in the shear zone and the country rock. Decreasing the stress exponent (to near one for superplastic flow) is therefore not conducive to strain localization (e.g. Bowden, 1970). There is absolutely no evidence in the detailed SEM images for the necessary large amount of grain boundary sliding and diffusive mass transfer required for granular flow. Indeed the marker lines provided by boudinaged rutile needles show that the amount of rotation between adjacent recrystallized small grains is small (Fig. 1d). The strong quartz CPO (Fig. 7) also argues for a deformation mechanism dominated by intracrystalline glide (largely on the prism ⟨*a*⟩ slip system).

As proposed by Pennacchioni and Cesare (1997), the synkinematic metamorphic paragenesis argues strongly for a water-deficient environment of the MM mylonites during shearing. Our observations of very low grain boundary porosity in the SEM images of broken surfaces clearly support this proposal. The results of this study suggest that the lack of a water-rich intragranular fluid wetting the grain boundaries strongly inhibits grain boundary mobility (e.g. Urai et al., 1986, Appendix) and therefore hinders recrystallization by grain boundary migration. The new grain microstructure is determined by the recrystallization mechanism, which in turn reflects competition between volume diffusion-controlled dislocation climb promoting polygonization/subgrain formation and grain boundary diffusion, important for grain boundary mobility. Grain boundary diffusion will be dramatically influenced by the amount and composition of any free-fluid phase. In the scheme proposed by Hirth and Tullis (1992), regime 1 is dominated by bulging recrystallization involving slow grain boundary migration. In regime 2, diffusion-controlled dislocation climb is fast enough to allow subgrain nucleation and rotation, and in regime 3, grain boundary migration dominates. The gradual transition between these regimes has generally been assigned to effects of temperature and/or strain rate (e.g. Stipp et al., 20002a,b). However, the data presented in this paper apparently does not fit this scheme (Fig. 9). We argue that the difference is due to the

water-deficient character of the MM mylonites. In this case, grain boundary mobility is very low, so that competing bulging and subgrain rotation recrystallization mechanisms continue to dominate at temperatures where they would usually be overwhelmed by fast grain boundary migration. Water-deficient conditions do not appear to have correspondingly influenced the intragranular glide mechanisms, since the CPO developed is the same as that measured in more typical water-rich amphibolite facies environments. An attempt to explain these results in terms of decreasing temperature during deformation could account for the finer grain size but could not explain the observed CPOs of the extensively recrystallized fine-grained samples. Even if it was argued that a strong precursor host control on new grain orientation (e.g. Pauli et al., 1996) allowed the high-temperature CPO to be maintained during subsequent lower-temperature deformation, this could not explain the observed stability of dynamically recrystallized An-rich plagioclase.

This study also indicates that high deviatoric stresses can be attained in the mid- to lower crust. For an angle of internal friction of 30° and a cohesion of 25 MPa, the necessary differential stress ($\Delta\sigma = \sigma_1 - \sigma_3$) for Mohr–Coulomb failure of dry rock at a confining pressure of 250–450 MPa is 300–500 MPa. Under the water-deficient conditions considered appropriate for the MM mylonites, the effective confining pressure should be close to lithostatic. The observed development of pseudotachylytes during shearing (Pennacchioni and Cesare, 1997) therefore implies that differential stress was indeed on the order of 300–500 MPa, at least during transient brittle failure. In a steady state condition, the recrystallized grain size is predicted to depend on the differential stress according to the relation

$$\frac{D}{b} = K_n\left(\frac{\Delta\sigma}{\mu}\right)^{-n} \quad (1)$$

where D is the grain size, b the Burgers of the dominant slip system, μ the elastic shear modulus, and K_n and n are constants (Twiss, 1977). The averaged elastic shear moduli for quartz is ca. 42 GPa and the Burgers vector is generally taken as $b = 0.5$ nm (Twiss, 1977; Kohlstedt and Weathers, 1980). Different authors have argued for somewhat differing values of K_n and n (e.g. see discussion in Kohlstedt and Weathers, 1980), but for quartzite the published values are generally close to the original values of $K_n = 4.60$ and $n = 1.47$ suggested by Twiss (1977) (e.g. see Gleason and Tullis, 1995). Using these values, a differential stress of 300–500 MPa would correspond to a recrystallized quartz grain size of 3.3–1.6 μm, which is within the range of $Qtz_{2,2}$ grain sizes actually observed in the MM mylonites (i.e. generally ≤5 μm, e.g. Fig 4c and d).

Recrystallization in itself is a strain-softening mechanism (e.g. Cahn, 1965; Poirier, 1985; Bystricky et al., 2000; Pieri et al., 2001) due to the elimination of dislocations hindering further dislocation glide and to the promotion of a strong CPO. Our results suggest that the availability of free water does not significantly affect the choice of active slip system(s), although experimental results clearly demonstrate that the flow stress for crystal plastic deformation of quartz decreases with increased amounts of added free water and with water fugacity (the 'hydrolytic weakening' effect, e.g. Blacic and Christie, 1984; Jaoul et al., 1984; Ord and Hobbs, 1986; Paterson, 1989; Kohlstedt et al., 1995). However, the presence or absence of a dispersed water-rich fluid on grain boundaries certainly does markedly influence grain boundary mobility (e.g. Urai et al., 1986; Spiers et al., 1988; Drury and Urai, 1990). Since recrystallization by grain boundary migration is the favoured mechanism under wet amphibolite facies conditions, suppression of this mechanism under dry conditions and the consequent preservation of finer grains with higher average dislocation densities would mean that the necessary differential stress for continued deformation would be higher than for a wet environment. This high differential stress, which from our observations can clearly be attained in the mid- to lower crust (10–20 km depth), is reflected in the fine recrystallized grain size and in transient brittle behaviour, with the development of pseudotachylytes. The low water activity and consequent low grain boundary mobility has also allowed the preservation of these fine-grained textures both during the continuing pre-Alpine history and the later Alpine overprint. Only where water had access during retrograde Alpine shearing were the microstructures subsequently destroyed.

7. Conclusions

The pre-Alpine Mont Mary mylonites developed under water-deficient upper amphibolite facies conditions (Pennacchioni and Cesare, 1997). However, they preserve a microstructure that is typical, under water-rich conditions, of lower grade greenschist facies deformation rather than amphibolite facies conditions, such as those illustrated from the Simplon Fault Zone. The CPOs of the samples, both high- and low-grade, more directly reflect the metamorphic conditions of deformation. It is argued, therefore, that the presence or absence of abundant water-rich fluid on the grain boundaries (1) is critical for grain boundary mobility, and therefore the transition from slow to fast grain boundary migration, but (2) has little influence on the mechanisms of intracrystalline dislocation glide and therefore CPO development. For water-deficient conditions, the restriction of grain boundary mobility hinders activity of the favoured recrystallization mechanism (namely grain boundary migration) and thereby limits the rate of recovery of strain-hardened microstructures (see discussion in Poirier (1985, p. 188)), with the result that the flow stress for ongoing deformation is higher. Marked weakening of such rocks only occurs with the introduction of water (e.g. in the later Alpine shear zones) or with the onset of partial melting (by further increase in temperature, by decompression, or

also by introduction of water). Water-deficient conditions actually appear to have been the norm in the currently exposed slices of the pre-Alpine basement and may also be typical of many other upper amphibolite to granulite facies basement units. Under such dry conditions, mid- to lower-crustal rocks may be quite strong, reaching differential stresses on the order of 300–500 MPa, and capable of brittle failure, now recorded in the MM examples as sheared pseudotachylytes in very fine grained quartz-feldspar mylonites.

Acknowledgements

Many thanks to Karsten Kunze, Jörg Bollmann and Richard Spiess for their considerable help with SEM imaging and to Karsten Kunze and Martin Schmocker for the texture goniometer analyses. We gratefully acknowledge the review of Janos Urai and especially the very thorough and constructive review of Jan Tullis. Part of the project was funded by the University of Padova (progetti di Ateneo; title of the project: Le zone di shear milonitico—uno strumento di interpretazione reologica).

References

Altenberger, U., Wilheim, S., 2000. Ductile deformation of K-feldspar in dry eclogite facies shear zones in the Bergen Arcs, Norway. Tectonophysics 320, 107–121.

Bailey, F.E., Hirsch, P.B., 1962. The recrystallization process in some polycrystalline metals. Proceedings of the Royal Society of London A267, 11–30.

Ballèvre, M., Kienast, J.-R., Vuichard, J.-P., 1986. La "nappe de la Dent-Blanche" (Alpes occidentales): Deux unités austroalpines indépendantes. Eclogae Helvetiae 79, 57–74.

Berthé, D., Choukroune, P., Jegouzo, P., 1979. Orthogneiss, mylonite and non-coaxial deformation of granites: the example of the South Armorican Shear Zone. Journal of Structural Geology 1, 31–42.

Blacic, J.D., Christie, J.M., 1984. Plasticity and hydrolitic weakening of quartz single crystals. Journal of Geophysical Research 89, 4223–4239.

Bowden, P.B., 1970. A criterion for inhomogeneous plastic deformation. Philosophical Magazine (Series 8) 22, 455–462.

Bucher, K., Frey, M., 1994. Petrogenesis of Metamorphic Rocks, 6th Ed, Springer, Heidelberg.

Burg, J.P., Laurent, P., 1978. Strain analysis of a shear-zone in a granodiorite. Tectonophysics 47, 15–42.

Bystricky, M., Kunze, K., Burlini, L., Burg, J.-P., 2000. High shear strain of olivine aggregates: rheological and seismic consequences. Science 290, 1564–1567.

Cahn, R.W., 1965. Recovery and recrystallization. In: Cahn, R.W., (Ed.), Physical Metallurgy, John Wiley & Sons, New York, pp. 925–987.

Canepa, M., Castelletto, M., Cesare, B., Martin, S., Zaggia, L., 1990. The Austroalpine Mont Mary Nappe (Italian Western Alps). Memorie di Scienze Geologiche 42, 1–17.

Debat, P., Sirieys, P., Deramont, J., Soula, J.C., 1975. Paleodéformations d'un massif orthogneissique. Tectonophysics 28, 159–183.

Den Brok, B., 1992. An experimental investigation into the effect of water on the flow of quartzite. Geologica Ultraiectina 95, 178pp.

Den Brok, S.W.J., 1998. Effect of microcracking on pressure-solution strain rate: the Gratz grain-boundary model. Geology 26, 915–918.

Den Brok, S.W.J., Spiers, C.J., 1991. Experimental evidence for water weakening of quartzite by microcracking plus solution-precipitation creep. Journal of the Geological Society, London 148, 541–548.

Drury, M.R., Urai, J.L., 1990. Deformation-related recrystallization processes. Tectonophysics 172, 235–253.

Dunlap, W.J., Hirth, G., Teyssier, C., 1997. Thermomechanical evolution of a ductile complex. Tectonics 16, 983–1000.

Etheridge, M.A., Wilkie, J.C., 1979. Grainsize reduction, grain boundary sliding, and the flow strength of mylonites. Tectonophysics 58, 159–178.

Fitz Gerald, J.D., Stünitz, H., 1993. Deformation of granitoids at low metamorphic grade. I: reaction and grain size reduction. Tectonophysics 221, 269–297.

Gleason, G.C., Tullis, J., 1995. A flow law for dislocation creep of quartz aggregates determined with the molten salt cell. Tectonophysics 247, 1–23.

Gleason, G.C., Tullis, J., Heidelbach, F., 1993. The role of dynamic recrystallization in the development of lattice preferred orientations in experimentally deformed quartz aggregates. Journal of Structural Geology 15, 1145–1168.

Grasemann, B., Mancktelow, N.S., 1993. Two-dimensional thermal modelling of normal faulting: the Simplon Fault Zone, Central Alps, Switzerland. Tectonophysics 225, 155–165.

Gratz, A.J., 1991. Solution-transfer compaction of quartzites: progress toward a rate law. Geology 19, 901–904.

Hacker, B.R., Yin, A., Christie, J.M., Snoke, A.W., 1990. Differential stress, strain rate, and temperatures of mylonitization in the Ruby Mountains, Nevada: implications for the rate and duration of uplift. Journal of Geophysical Research 95, 8569–8580.

Hacker, B.R., Yin, A., Christie, J.M., Davis, G.A., 1992. Stress magnitude, strain rate and rheology of extended middle continental crust inferred from quartz grain sizes in the Whipple Mountains, California. Tectonics 11, 36–46.

Hippertt, J.F.M., 1994a. Direct observation of porosity in quartzite and phyllonite. Neues Jahrbuch für Mineralogie-Abhandlungen 166, 239–259.

Hippertt, J.F.M., 1994b. Grain boundary microstructures in micaceous quartzite: significance of fluid movement and deformation processes in low metamorphic grade shear zones. Journal of Geology 102, 331–348.

Hirth, G., Tullis, J., 1992. Dislocation creep regimes in quartz aggregates. Journal of Structural Geology 14, 145–159.

Jaoul, O., Tullis, J., Kronenberg, A., 1984. The effect of varying water contents on the creep behavior of Heavitree quartzite. Journal of Geophysical Research 89, 4298–4312.

Kleinschrodt, R., Duyster, J.P., 2002. HT-deformation of garnet: an EBSD study on granulites from Sri Lanka, India and the Ivrea Zone. Journal of Structural Geology 24, 1829–1844.

Kohlstedt, D.L., Weathers, M.S., 1980. Deformation-induced microstructures, paleopiezometers, and differential stresses in deeply eroded fault zones. Journal of Geophysical Research 85, 6269–6285.

Kohlstedt, D.L., Evans, B., Mackwell, S.J., 1995. Strength of the lithosphere: constraints imposed by laboratory experiments. Journal of Geophysical Research 100, 17587–17602.

Kretz, R., 1983. Symbols for rock-forming minerals. American Mineralogist 68, 277–279.

Kronenberg, A.K., Tullis, J., 1984. Flow strengths of quartz aggregates: grain size and pressure effects due to hydrolytic weakening. Journal of Geophysical Research 89, 4281–4297.

Kruse, R., Stünitz, H., Kunze, K., 2000. Dynamic recrystallization processes in plagioclase porphyroclasts. Journal of Structural Geology 23, 1781–1802.

Law, R.D., 1986. Relationships between strain and quartz crystallographic fabrics in the Roche Maurice quartzites of Plougastel, western Brittany. Journal of Structural Geology 8, 493–515.

Law, R.D., 1987. Heterogeneous deformation and quartz crystallographic fabric transitions: natural examples from the Moine Thrust zone at the

Stack of Glencoul, northern Assynt. Journal of Structural Geology 9, 819–833.

Law, R.D., 1990. Crystallographic fabrics: a selective review of their applications to research in structural geology. In: Knipe, R.J., Rutter, E.H. (Eds.), Deformation Mechanisms, Rheology and Tectonics, Geological Society Special Publication 54, pp. 335–352.

Law, R.D., Knipe, R.J., Dayan, H., 1984. Strain path partitioning within thrust sheets: microstructural and petrofabric evidence from the Moine Thrust zone at Loch Eriboll, northwest Scotland. Journal of Structural Geology 6, 477–497.

Law, R.D., Casey, M., Knipe, R.J., 1986. Kinematic and tectonic significance of microstructures and crystallographic fabrics within quartz mylonites from the Assynt and Eriboll regions of the Moine thrust zone, NW Scotland. Transactions of the Royal Society of Edinburgh 77, 99–125.

Lister, G.S., 1977. Discussion: crossed girdle c-axis fabrics in quartzites plastically deformed by plane strain and progressive simple shear. Tectonophysics 39, 51–54.

Lister, G.S., Price, G.P., 1978. Fabric development in a quartz-feldspar mylonite. Tectonophysics 49, 37–78.

Mackinnon, P., Fueten, F., Robin, P.-Y., 1997. A fracture model for quartz ribbons in straight gneisses. Journal of Structural Geology 19, 1–14.

Mancktelow, N.S., 1985. The Simplon Line: a major displacement zone in the western Lepontine Alps. Eclogae Geologicae Helvetiae 78, 73–96.

Mancktelow, N.S., 1987a. Quartz textures from the Simplon Fault Zone, southwest Switzerland and north Italy. Tectonophysics 135, 133–153.

Mancktelow, N.S., 1987b. Atypical textures in quartz veins from the Simplon Fault Zone. Journal of Structural Geology 9, 995–1005.

Mancktelow, N.S., 1990. The Simplon Fault Zone. Beiträge zur Geologischen Karte der Schweiz [Neue Folge] 163, 74.

Mancktelow, N.S., Grujic, D., Johnson, E.L., 1998. An SEM study of porosity and grain boundary microstructure in quartz mylonites, Simplon Fault Zone, Central Alps. Contributions to Mineralogy and Petrology 131, 71–85.

Means, W.D., 1981. The concept of a steady state foliation. Tectonophysics 78, 179–199.

Musumeci, G., 2002. Sillimanite-bearing shear zones in syntectonic leucogranite: fluid-assisted brittle-ductile deformation under amphibolite facies conditions. Journal of Structural Geology 24, 1491–1505.

Olsen, T.S., Kohlstedt, D.L., 1985. Natural deformation and recrystallization of some intermediate plagioclase feldspars. Tectonophysics 111, 107–131.

Ord, A., Christie, J.M., 1984. Flow stresses from microstructures in mylonitic quartzites of the Moine thrust zone, Assynt area, Scotland. Journal of Structural Geology 6, 639–654.

Ord, A., Hobbs, B.E., 1986. Experimental control of the water-weakening effect in quartz. In: Hobbs, B.E., Heard, H.C. (Eds.), Mineral and Rock Deformation: Laboratory Studies. The Paterson Volume. Geophysical Monograph 36, pp. 51–72, American Geophysical Union, Washington, DC.

Passchier, C.W., 1982. Mylonitic deformation in the Saint-Bathélemy massif, French Pyrenees, with emphasis on the genetic relationship between ultramylonite and pseudotachylyte. GUA Papers of Geology, Series 1, 16-1982, 173pp.

Passchier, C.W., 1985. Water-deficient mylonite zones—an example from the Pyrenees. Lithos 18, 115–127.

Paterson, M.S., 1989. The interaction of water with quartz and its influence in dislocation flow—an overview. In: Karato, S.-I., Toriumi, M. (Eds.), Rheology of Solids and of the Earth, Oxford Science Publications, Oxford, pp. 107–142.

Pauli, C., Schmid, S.M., Panozzo Heilbronner, R., 1996. Fabric domains in quartz mylonites: localized three dimensional analysis of microstructure and texture. Journal of Structural Geology 18, 1183–1203.

Pennacchioni, G., Cesare, B., 1997. Ductile-brittle transition in pre-Alpine amphibolite facies mylonites during evolution from water-present to water-deficient conditions (Mont Mary Nappe, Italian Western Alps). Journal of Metamorphic Geology 15, 777–791.

Pennacchioni, G., Guermani, A., 1993. The mylonites of the Austroalpine Dent Blanche Nappe along the northwestern side of the Valpelline Valley (Italian Western Alps). Memorie di Scienze Geologiche 45, 37–55.

Pieri, M., Burlini, L., Kunze, K., Stretton, I., Olgaard, D.L., 2001. Rheological and microstructural evolution of Carrara marble with high shear strain: results from high temperature torsion experiments. Journal of Structural Geology 23, 1393–1413.

Poirier, J.-P., 1985. Creep of Crystals, Cambridge University Press, Cambridge.

Poirier, J.-P., Nicolas, A., 1975. Deformation-induced recrystallization due to progressive misorientation of subgrains, with special reference to mantle peridotites. Journal of Geology 83, 707–720.

Pryer, L.L., 1993. Microstructures in feldspars from a major crustal thrust zone: the Grenville Front, Ontario, Canada. Journal of Structural Geology 15, 21–36.

Pryer, L.L., Robin, P.-Y.F., 1995. Retrograde metamorphic reactions in deforming granites and the origin of flame perthite. Journal of Metamorphic Geology 13, 645–658.

Ramsay, J.G., Allison, I., 1979. Structural analysis of shear zones in an alpinised Hercynian granite (Maggia Lappen, Pennine Zone, Central Alps). Schweizerische Mineralogische und Petrographische Mitteilungen 59, 251–279.

Schmid, S.M., Casey, M., 1986. Complete fabric analysis of some commonly observed quartz c-axis patterns. In: Hobbs, B.E., Heard, H.C. (Eds.), Mineral and Rock Deformation: Laboratory Studies. The Paterson Volume. Geophysical Monograph 36, pp. 263–286. American Geophysical Union, Washington, DC.

Sibson, R.H., White, S., Atkinson, B.K., 1979. Fault rock distribution and structure within the Alpine Fault Zone: a preliminary account. In: Walcot, R.I., Cresswell, M.M. (Eds.), The Origin of the Southern Alps. Bulletin of the Royal Society of New Zealand 18, pp. 55–66.

Simpson, C., Schmid, S.M., 1983. An evaluation of criteria to deduce the sense of movement in sheared rocks. Geological Society of America Bulletin 94, 1281–1288.

Spiers, C.J., Urai, J.L., Lister, G.S., 1988. The effect of brine (inherent or added) on rheology and deformation mechanisms in salt rock. In: Hardy, H.R., Langer, M. (Eds.), The Mechanical Behaviour of Salt: Proceedings of the Second Conference, Trans Tech Publications, Clausthal-Zellerfeld, pp. 89–102.

Stipp, M., Stünitz, H., Heilbronner, R., Schmid, S.M., 2002. Dynamic recrystallization of quartz: correlation between natural and experimental conditions. In: De Meer, S., Drury, M.R., De Bresser, J.H.P., Pennock, G.M. (Eds.), Deformation Mechanisms, Rheology and Tectonics: Current Status and Future Perspectives. Geological Society, London, Special Publications 200, pp. 171–190.

Stipp, M., Stünitz, H., Heilbronner, R., Schmid, S.M., 2002b. The eastern Tonale fault zone: a 'natural laboratory' for crystal plastic deformation of quartz over a temperature range from 250 to 700 °C. Journal of Structural Geology 24, 1861–1884.

Stöckhert, B., Brix, M.R., Kleinschrodt, R., Hurford, A.J., Wirth, R., 1999. Thermochronometry and microstructures of quartz—a comparison with experimental flow laws and predictions on the temperature of the brittle-plastic transition. Journal of Structural Geology 21, 351–369.

Tullis, J., Yund, R.A., 1987. Transition from cataclastic flow to dislocation creep of feldspar: mechanisms and microstructures. Geology 15, 606–609.

Tullis, J., Yund, R.A., 1989. Hydrolytic weakening of quartz aggregates: the effects of water and pressure on recovery. Geophysical Research Letters 16, 1343–1346.

Twiss, R.J., 1977. Theory and applicability of a recrystallized grain size paleopiezometer. Pure and Applied Geophysics 115, 227–244.

Urai, J.L., Means, W.D., Lister, G.S., 1986. Dynamic recrystallization of minerals. In: Hobbs, B.E., Heard, H.C. (Eds.), Mineral and Rock Deformation: Laboratory Studies. The Paterson Volume. Geophysical Monograph 36, pp. 161–199, American Geophysical Union, Washington, DC.

Van Daalen, M., Heilbronner, R., Kunze, K., 1999. Orientation analysis of localized shear deformation in quartz fibres at the brittle-ductile transition. Tectonophysics 303, 83–107.

Vernon, R.H., 1999. Flame perthite in metamorphic gneisses at Cooma, SE Australia. American Mineralogist 84, 1760–1765.

Vidal, J.-L., Kubin, L., Debat, P., Soula, J.-C., 1980. Deformation and dynamic recrystallization of K feldspar augen in orthogneiss from Montagne Noire, Occitania, Southern France. Lithos 13, 247–255.

Weathers, M.A., Bird, J.M., Cooper, R.F., Kohlstedt, D.L., 1979. Differential stress determined from deformation-induced microstructures of the Moine Thrust Zone. Journal of Geophysical Research 84, 7495–7509.

Winkler, H.G.F., 1979. Petrogenesis of Metamorphic Rocks, Springer-Verlag, New York.